Aus dem Institut für Neurophysiologie
der Medizinischen Fakultät Charité – Universitätsmedizin Berlin

DISSERTATION

Connectivity and Dynamics Underlying Synaptic Control of the Subthalamic Nucleus
-
Konnektivität und Dynamik der Synaptischen Kontrolle des Nucleus Subthalamicus

zur Erlangung des akademischen Grades
Medical Doctor - Doctor of Philosophy (MD/PhD)

vorgelegt der Medizinischen Fakultät
Charité – Universitätsmedizin Berlin

von

Leon Amadeus Steiner
aus Berlin

Datum der Promotion: 18.12.2020

TABLE OF CONTENTS

LIST OF FIGURES

LIST OF TABLES

LIST OF ABBREVIATIONS

µm	micrometer
aDBS	adaptive deep brain stimulation
AP	action potential
Cat#	catalogue number
CCM	Charité Campus Mitte
CPP	3-(2-Carboxypiperazin-4-yl)propyl-1-phosphonic acid
DBS	deep brain stimulation
EPSC	excitatory postsynaptic current
GABA	gamma aminobutyric acid
GPe	external Globus Pallidus
GPi	internal Globus Pallidus
HFS	high frequency stimulation
Hz	herz
ICMJE	International Committee of Medical Journal Editors
M1	primary motor cortex
ms	millisecond
Na^+	sodium
NBQX	1,2,3,4-Tetrahydro-6-nitro-2,3-dioxo-benzoquinoxaline-7-sulfonamide
NGO	non governmental organisation
PD	Parkinson's Disease
s	second
SEM	standard error of the mean
SNr	Substantia Nigra pars reticulata
STN	Subthalamic Nucleus
Str	Striatum
THS	Tiefe Hirnstimulation
UCL	University College London
UK	United Kingdom
URM	uniform requirements for manuscripts
vGAT	vesicular GABA transporter
YFP	yellow fluorescent protein

(1) ABSTRACTS

1.1 Abstract (English)

The Subthalamic Nucleus (STN) is part of the basal ganglia, integrates glutamatergic cortical (hyperdirect) and pallidal GABAergic (indirect) inputs and projects to all output structures of the basal ganglia. As a target of deep brain stimulation (DBS), the STN is of clinical interest to treat symptoms of Parkinson's Disease.

Dynamics of neuronal synchronization in the STN have been shown to shape the nucleus` function in both health and disease and to be directly modulated by therapeutic DBS. Yet knowledge of intrinsic and afferent STN connectivity, which may underlie the synaptic control of STN neuronal synchronization, is limited.

In this study, we investigate connectivity rules in the rat STN by means of simultaneous multiple-cell patch-clamp recordings in combination with extracellular electrical stimulation and neuroanatomical analysis.

In terms of intrinsic connectivity, our findings suggest a lack of mutual synaptic connections between STN neurons. Analysis of afferent connectivity revealed a sparse and selective innervation of local clusters of STN neurons by both glutamatergic and GABAergic fibers. Activation of glutamatergic input in isolation resulted in highly synchronous recruitment of STN neurons, whereas co-stimulation of GABAergic input delayed and desynchronized action potential (AP) generation. While extracellular electrical stimulation at low frequencies depressed both glutamatergic and GABAergic inputs to a similar degree, DBS-like frequencies of 130 Hz resulted in a significantly stronger depression of glutamatergic inputs compared to depression of GABAergic inputs. Recovery from short-term depression was complete at both GABAergic and glutamatergic synapses within seconds.

In summary, our findings indicate that STN neurons operate as parallel processing units. Hence, synchronization of local clusters of neurons in the STN is likely to depend on upstream structures, interacting with the STN via sparse and specific synaptic single fiber input. The vulnerability of glutamatergic input to synaptic depression at DBS-like frequencies suggests a DBS mechanism of action that is based on a decoupling of the STN from direct cortical synchronization and a shift to desynchronizing GABAergic input. This may contribute to the effect of electrical stimulation, counteracting exaggerated neuronal synchronization in Parkinson's Disease. Together, the rapid time course of differential short-term depression at high stimulation frequencies and the subsequent fast

synaptic recovery provide assets for a moment-to-moment control of neuronal synchrony that next-generation DBS aims for.

1.2 Abstract (German)

Der Nucleus Subthalamicus (STN) ist Teil der Basalganglien, integriert glutamaterge, kortikale (hyperdirekter Pfad) und GABAerge, pallidale (indirekter Pfad) Eingänge und ist direkt mit allen Ausgangstrukturen der Basalganglien verschaltet. Als Zielstruktur der Tiefen Hirnstimulation (THS) ist er von klinischem Interesse für die symptomatische Therapie des Morbus Parkinson.

Neuronale Synchronisationsdynamiken bestimmen die Funktion des STN in physiologischen und pathologischen Zuständen und werden durch therapeutisch wirksame THS direkt moduliert. Dennoch ist das Wissen über synaptische Verschaltungsprinzipien der intrinsischen und afferenten Konnektivität, die solchen Synchronisationsdynamiken zugrunde liegen, beschränkt. In dieser Studie untersuchen wir synaptische Verschaltungsprinzipien im STN der Ratte mittels simultaner multipler Patch-Clamp Ableitungen in Kombination mit extrazellulärer elektrischer Stimulation und neuroanatomischer Analyse.

Bezüglich intrinsischer Konnektivität legen unsere Ergebnisse nahe, dass es keine direkten synaptischen Verbindungen zwischen STN Neuronen gibt. Die Analyse der afferenten Verschaltungsmuster zeigte eine selektive Innervation lokaler Cluster von STN-Neuronen durch glutamaterge und GABAerge Fasern. Aktivierung von glutamatergen Afferenzen in Isolation löste eine hochsynchrone Rekrutierung von STN-Neuronen aus, während eine Co-Stimulation GABAerger Eingänge zu einer Verzögerung und Desynchronisation der generierten Aktionspotentiale führte. Während die synaptische Kurzzeitdepression für glutamaterge und GABAerge Eingänge bei niedrigfrequenter extrazellulärer elektrischer Stimulation vergleichbar war, führten THS-ähnliche Stimulationsfrequenzen von 130 Hz zu einer signifikant stärkeren Kurzzeitdepression glutamaterger im Vergleich zu GABAergen Eingängen. Die synaptische Depression sowohl glutamaterger als auch GABAerger Eingänge zeigte sich innerhalb von Sekunden reversibel.

Zusammenfassend legen die Ergebnisse dieser Studie nahe, dass STN Neurone als parallele Prozessierungseinheiten operieren. Somit hängt die Synchronisation lokaler Cluster von STN Neuronen mutmaßlich von vorgeschaltenen Regionen ab, die über selektive Verschaltungen mit dem STN interagieren. Die Vulnerabilität glutamaterger Transmission bei THS-ähnlichen Stimualtionsfrequenzen impliziert eine Abkopplung von direkter kortikaler Synchronisierung, während zeitgleich eine Verschiebung hin zu desynchronisierenden GABAergen Eingängen stattfindet. Dies trägt möglicherweise zu

einer Suppression pathologisch erhöhter neuraler Synchronität, wie sie beim Morbus Parkinson vorkommt, bei. Zusammen stellen der rapide zeitliche Verlauf der differenziellen Kurzzeitplastizität bei hohen Stimulationsfrequenzen und die darauffolgende schnelle synaptische Erholung Voraussetzungen einer zeitlich präzisen Kontrolle neuronaler Synchronität im STN dar, die bei Weiterentwicklungen der THS angestrebt wird.

(2) INTRODUCTION

Movement control critically depends on dynamic interactions between structures of the cortex-basal ganglia loops. Among the subcortical nuclei that participate in this circuitry, the Subthalamic Nucleus (STN) is the only glutamatergic structure and it directly controls basal ganglia-output nuclei (Synopsis Figure 1). Integrating cortical glutamatergic (hyperdirect pathway) and pallidal GABAergic (indirect pathway) input, the STN thus occupies a key position to participate in the initiation, execution, and termination of movement sequences (Nambu et al., 2002). Neuronal processing of such motor control comprises brief bursts of neuronal synchronization at beta frequencies (13-35 Hz) (Mirzaei et al., 2017; Tinkhauser et al., 2017a).

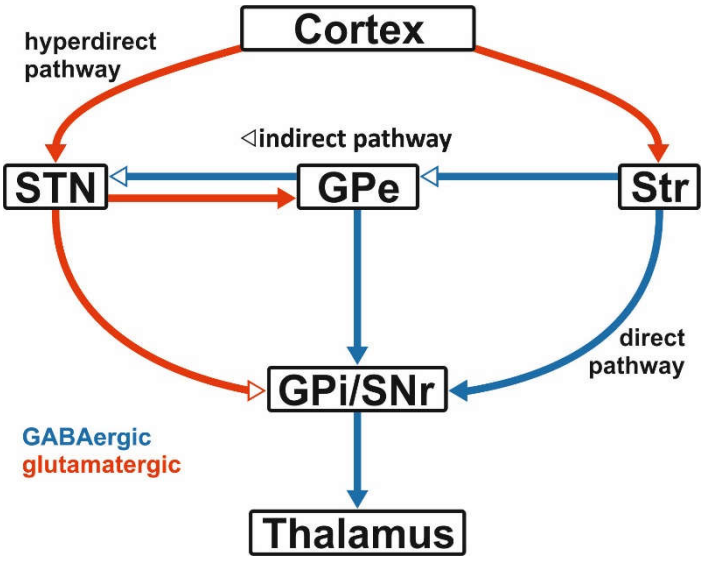

Synopsis Figure 1. Scheme of the hyperdirect (Cortex to STN), direct (Str to GPi), and indirect (Str to GPe to STN to GPi) pathways. Glutamatergic and GABAergic connections are marked red and blue, respectively. Empty arrows mark the indirect pathway. STN, Subthalamic Nucleus; GPe, external Globus Pallidus; Str, Striatum; GPi, internal Globus Pallidus; SNr, Substantia Nigra pars reticulata.

Dynamics of neuronal synchrony shape STN function in health (Mirzaei et al., 2017) and predict pathophysiological states in movement disorders such as Parkinson's Disease (PD) (Tinkhauser et al., 2017a). Furthermore, dynamics of neuronal synchrony represent the target in next-generation approaches of deep brain stimulation (DBS), that aim to interact with ongoing synchronization dynamics in a timely precise manner (adaptive DBS, aDBS) (Little et al., 2013; Ramirez-Zamora et al., 2017; Tinkhauser et al., 2017b). Despite the suggested physiological and pathophysiological importance of neuronal synchronization dynamics in the STN, little is known about how such transient patterns of synchrony emerge.

Neuronal synchrony in the STN can be expected to be controlled by a specific pattern of intrinsic and / or afferent synaptic connectivity. More specifically, functional wiring of STN neurons may be related to STN synchrony in any of the following ways (for illustration see Synopsis Figure 2):

Hypothesis (A): Intranuclear mutual connectivity promotes the emergence of intrinsic synchrony.

Hypothesis (B): Divergent connectivity of single afferent fibers causes the synchronous recruitment of STN neurons.

Hypotheses (C & D): Coordinated activity of presynaptic structures up-stream of the STN interacting with the STN via sparse and selective input.

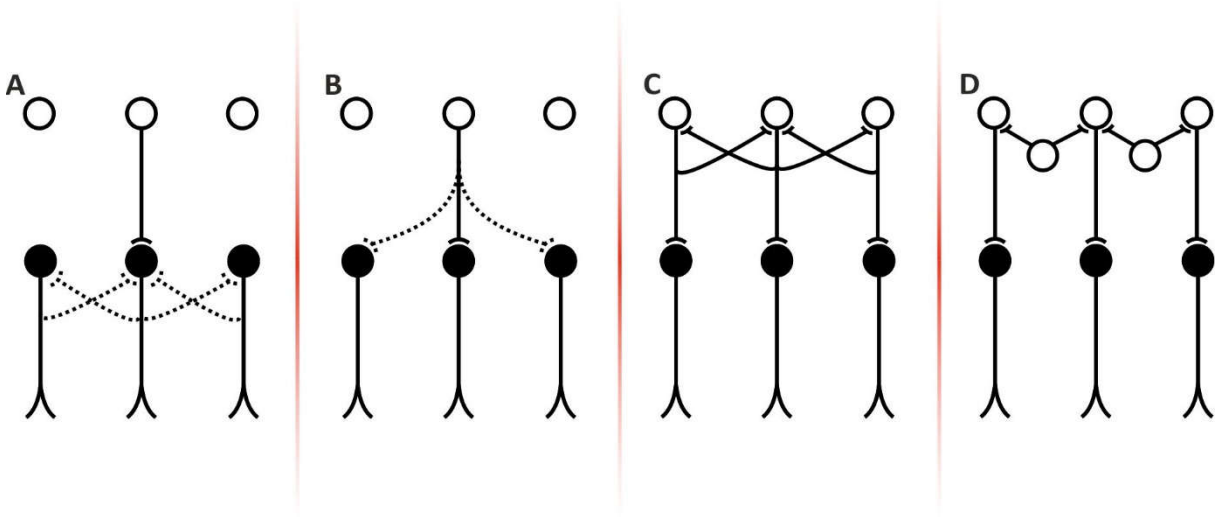

Synopsis Figure 2. Schemes illustrating plausible rules of intrinsic and afferent connectivity that may allow for STN synchronization (see text for detailed descriptions). Empty circles represent somata of neurons afferent to the STN (e.g. in Cortex or GPe). Filled circles represent somata of STN neurons.

Previous studies provide (indirect) evidence for each of the described scenarios:

(A) Suggestions for mutual synaptic connectivity between glutamatergic STN neurons have come from three lines of evidence: First, anatomical studies have shown intranuclear axon-collaterals of STN neurons (Hammond and Yelnik, 1983; Kita et al., 1983), which might serve as presynaptic sites for synaptic connections. However, no postsynaptic neurons have been identified in these studies. Second, computational models have predicted a minimum of 3% mutual synaptic connectivity between STN neurons (Gillies and Willshaw, 2004). Finally, complex excitatory postsynaptic currents (EPSCs) have been recorded in structures receiving projections from the STN following the electrical stimulation of the STN and have been interpreted as indirect proof for the existence of polysynaptic circuits between STN neurons (Shen and Johnson, 2006).

However, no paired patch-clamp recordings, which could ultimately prove functional synaptic interconnectivity between STN neurons, have been performed to date and evidence from other experimental approaches has questioned the existence or relevance of intrinsic synaptic connectivity in the STN (Wilson et al., 2004; Koshimizu et al., 2013).

(B) Afferent connectivity to the STN by single GABAergic fibers arising from the Globus Pallisus externus (GPe) has been suggested to be sparse and selective rather than broad and divergent (Baufreton et al., 2009). Similarly, the cortico-STN projection, conceptualized as the hyperdirect pathway, has been shown to consist of axonal collaterals of corticofugal projections that form sparse terminal fields in the STN (Kita and Kita, 2012; Coude et al., 2018). Although the aforementioned anatomical evidence suggests selective rather than divergent input by incoming fibers, functional connectivity of afferent fibers to local clusters of STN neurons has not been directly assessed. Single afferent fibers might project to single cells (selective single fiber input) or several cells (divergent single fiber input) within a given cluster (Synopsis Figure 3C). The latter may serve to synchronously recruit targeted cells, thus contributing to the emergence of STN synchrony without the necessity for prior synchronization in the presynaptic structure.

(C & D) The suggested restricted connectivity of GABAergic fibers to the STN has led to the conclusion that there has to be prior synchronization of GPe neurons in order for the GPe-STN connection to contribute to the synchronization of STN neurons (Baufreton et al., 2009). In addition to GABAergic inhibition, cortical excitation has been proposed to contribute to synaptic control of neuronal synchrony in the STN (Tachibana et al., 2011; Sanders and Jaeger, 2016). Previous work indicates that GABAergic inhibition occurring in anti-phase to glutamatergic input may further strengthen synchrony forwarded by cortical excitation (Baufreton et al., 2005). This adds support to the necessity of coordinated activity of cortex-basal ganglia loops to produce STN synchrony. Despite the possible importance of the interplay between neuronal structures for STN synchrony, knowledge of the interactions of the GABAergic and the glutamatergic input in the control of STN synchrony is limited and synaptic dynamics of GABAergic and glutamatergic inputs in response to high frequency stimulation (HFS) in the STN (the default DBS configuration) have not been directly compared.

In summary, key questions concerning synaptic connectivity within the STN remain unresolved. This motivates rigorous testing of the suggested patterns of intrinsic and afferent synaptic connectivity (Synopsis Figure 2). This study analyses connectivity rules in the STN by means of simultaneous multiple-cell patch-clamp recordings in combination with extracellular stimulation and neuroanatomical analysis. Further experiments examine the interactions of synaptic inputs to local clusters of STN neurons and compare synaptic dynamics of glutamatergic and GABAergic inputs in response to extracellular stimulation at low and high, DBS-like frequencies.

(3) METHODS complementing the publication

For a detailed description of the methods and experimental paradigms, please refer to Steiner et al., 2019. Below, additional information on key resources and a more detailed description of the multi-patch experimental paradigm are provided.

3.1 Table of key resources

REAGENT or RESOURCE	SOURCE	IDENTIFIER
Antibodies		
Streptavidin-Alexa Flour 647	Thermo Fisher Scientific	Cat# S32357
Chemicals, Peptides, and Recombinant Proteins		
Sucrose	Sigma-Aldrich	Cat# S1888
Potassium chloride (KCl)	Sigma-Aldrich	Cat# P9333
Sodium dihydrogen phosphate (NaH2PO4)	Carl Roth	Cat# T878.2
Glucose	Carl Roth	Cat# HN06.3
Sodium bicarbonate (NaHCO3)	Sigma-Aldrich	Cat# S5761
Calcium chloride (CaCl2)	Carl Roth	Cat# 5239.1
Magnesium chloride (MgCl2)	Carl Roth	Cat# 2189.1
Sodium chloride (NaCl)	Carl Roth	Cat# 9256.2
Potassium gluconate (K-gluconate)	Sigma-Aldrich	Cat# G4500
4-(2-hydroxyethyl)-1-piperazineethanesulfonic acid (HEPES)	Sigma-Aldrich	Cat# H3375
Ethylene glycol-bis(β-aminoethyl ether)-N,N,N',N'-tetraacetic acid (EGTA)	Sigma-Aldrich	Cat# E3889
Sodium phosphocreatine (Na2- phosphocreatine)	Sigma-Aldrich	Cat# P7936
Adenosine 5′-triphosphate disodium salt hydrate (Na2ATP)	Sigma-Aldrich	Cat# A9187
Guanosine 5′-triphosphate sodium salt hydrate (Na2GTP)	Sigma-Aldrich	Cat# G8877
Potassium hydroxide (KOH)	Carl Roth	Cat# K017.1
Gabazine	TOCRIS	Cat# 1262
D-AP5	TOCRIS	Cat# 0106
CNQX disodium salt	TOCRIS	Cat# 1045
Biocytin	Biomol	Cat# ABD-3080
Triton X-100	Carl Roth	Cat# 3051.3
Experimental Models: Organisms		
Rat: W-Tg(Slc32a1-YFP*)1Yyan	The National BioResource Project of the Rat in Japan	NBRP Rat No 0554
Software and Algorithms		
Clampfit (10.7.0.3)	Molecular Devices	N/A
Microsoft Excel (Microsoft Office Professional Plus 2013)	Microsoft Cooperation	RRID:SCR_016137
MATLAB (R2015b)	The Mathworks	RRID:SCR_001622
ImageJ (1.48)	NIH	RRID:SCR_003070
Neuron (7.4)	Yale University, Duke University	N/A

Synopsis Table 1. Table of key resources.

3.2 The multipatch-approach to study intrinsic and afferent connectivity

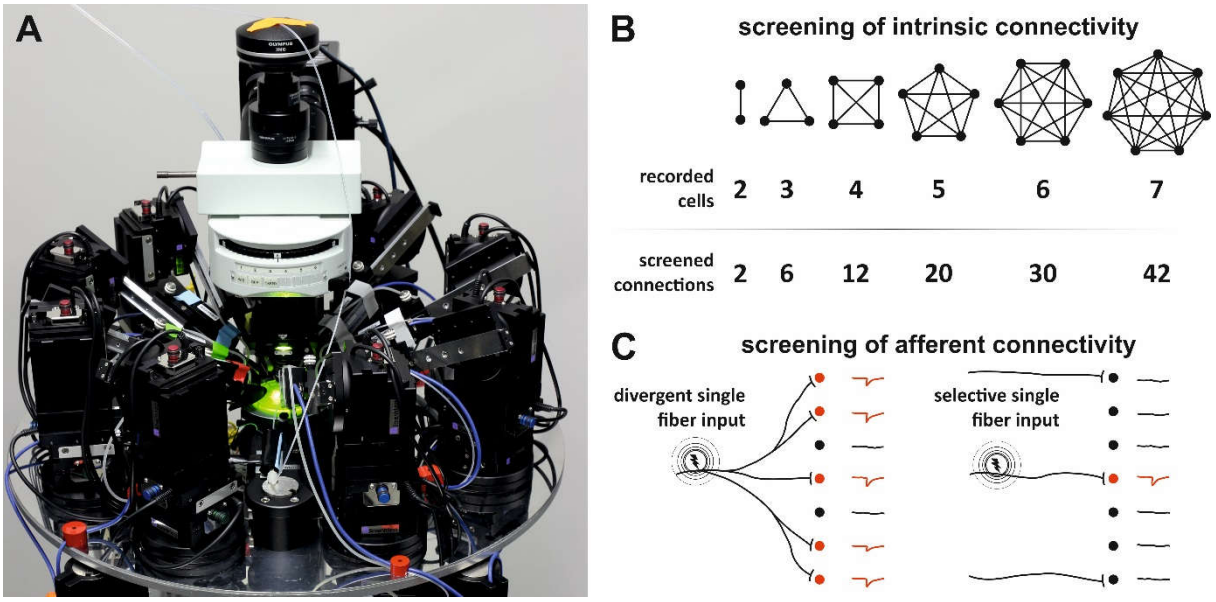

Synopsis Figure 3. The multipatch-approach to study intrinsic and afferent connectivity. (A) Photograph of the experimental set-up featuring eight micromanipulators (seven for patch-pipettes, one for extracellular stimulation); (B) Screening of intrinsic connectivity: Scheme illustrates how increasing the number of simultaneously recorded neurons (black dots) in individual experiments significantly increases the efficiency of screening for synaptic connections (connecting lines). (C) Screening of afferent connectivity: Scheme illustrates how the combination of multi-patch recordings and extracellular stimulation can aid to differentiate divergent and selective single fiber input to local clusters of neurons. Schematic drawings of afferent fibers; flash to illustrate extracellular electric stimulation; schematic postsynaptic traces illustrate read-out in whole-cell voltage clamp recordings. (A) and (B) were adapted from Peng et al., 2019.

To screen for synaptic connectivity, simultaneous multiple-neuron patch-clamp recordings represent a highly efficient experimental approach. Given their subthreshold and high temporal resolution, parallel patch-clamp recordings allow for the detection of both glutamatergic and GABAergic synaptic connections as small as 40 µV in average amplitude (Geiger et al., 1997). Furthermore, the whole-cell access to entire cell clusters enables detailed neuroanatomical analysis of the recorded clusters.

Increasing the number of simultaneously recorded cells directly translates into a significant increase in synaptic connections screened in each individual experiment (Synopsis Figure 3A and B), according to

$$c = n \times (n-1)$$

with c := screened connections in an individual experiment and n := number of simultaneously recorded neurons in the respective experiment

Due to the high efficiency of the multi-patch paradigm, fewer experiments are required to achieve comparable sample sizes (Peng et al., 2019).

Combining the multi-patch approach with extracellular stimulation represents a novel experimental approach to investigate afferent connectivity of the STN (Synopsis Figure 3C). Extracellular electric stimulation was applied using minimal stimulation strategies in order to analyze how single afferent fibers connect to local clusters of STN neurons. Specifically, divergence of afferents onto STN neurons within a recorded cluster was studied by assessing the parallel emergence of postsynaptic responses in simultaneously recorded cells at threshold stimulation intensity (Figure 4, Steiner et al., 2019).

(4) SUPPLEMENTARY RESULTS to the publication

For a detailed report of the results of this study please refer to Steiner et al., 2019. The following will provide supplementary information and figures not included in the corresponding publication.

Overview of supplemental material and link to the publication:

	Corresponding figure in Steiner et al., 2019
Supplementary Figure 1 Connectivity screening experiment in primary motor cortex (M1) as a control experiment	Figure 2B
Supplementary Figure 2 Axo-dendritic and axo-axonic proximities of STN neurons do not translate into functional synaptic connectivity between respective cells	Figure 2 and 3
Supplementary Figure 3 The rat STN represents a vGAT-negative structure	Figure 1D
Supplementary Figure 4 Patterns of spontaneous activity observed in the sample of STN neurons examined	Figure 1C

Synopsis Table 2. Overview of supplemental material and link to the publication.

4.1 Supplementary Figure 1: Connectivity screening experiment in primary motor cortex (M1) as a control experiment

The extensive connectivity screening between STN neurons reported on in Steiner et al., 2019 suggests a lack of mutual synaptic connectivity between the STN neurons. To validate the used approach of connectivity screening, control experiments were performed in other brain regions that are known to show high levels of connectivity. Supplementary Figure 1 (Synopsis Figure 4) shows a highly connected cell cluster in primary motor cortex (M1, layer 2/3) recorded under the same conditions as in experiments shown in the manuscript. The recording features a local inhibitory interneuron that projects to three principal cells and synaptic connectivity between the glutamatergic principal cells.

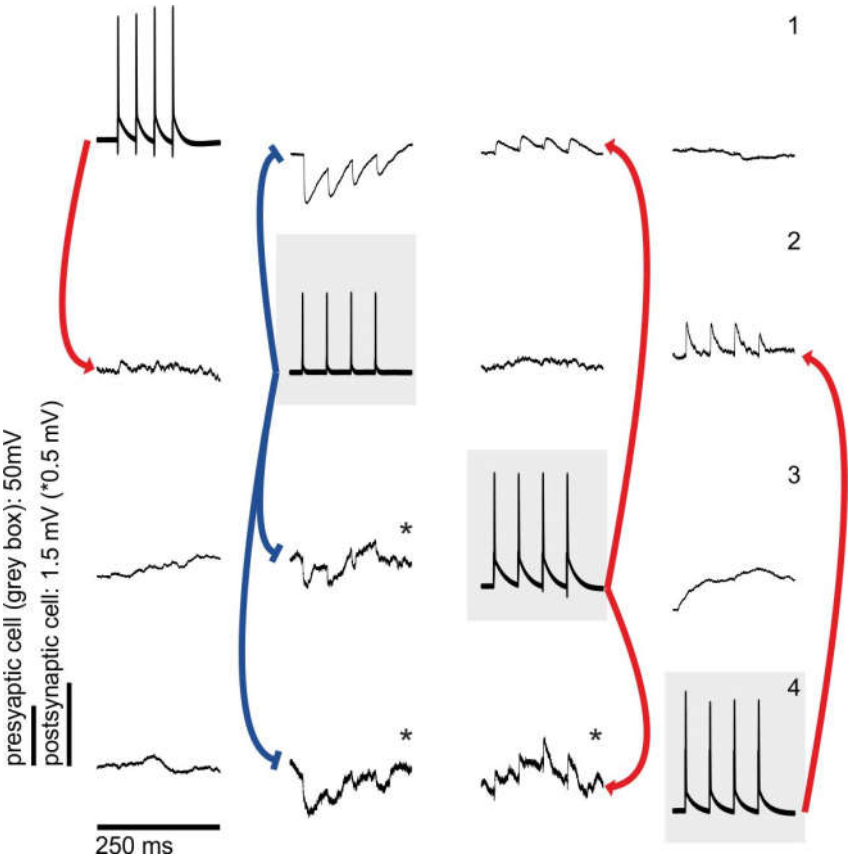

Synopsis Figure 4. Supplementary Figure 1 (linked to Figure 2B of Steiner et al., 2019).
Each neuron is consecutively stimulated to elicit 4 action potentials (gray boxes) in current-clamp mode. Simultaneous recordings of putative postsynaptic cells are shown in the same column. 30 sweep average shown. Excitatory and inhibitory synaptic connections are indicated by red and blue lines, respectively. Asterisks mark traces with varied vertical scale bar.

4.2 Supplementary Figure 2: Axo-dendritic and axo-axonic proximities of STN neurons do not translate into functional synaptic connectivity between respective cells

Consistent with previous studies, Steiner et al., 2019 (Figure 3) confirms the existence of intranuclear axon-collaterals in STN neurons and extends previous neuroanatomical findings providing stainings of both the putative presynaptic cell (axon-collateral) and the putative postsynaptic cell (dendrites of other STN neuron within a stained cluster). Spatial proximities between STN neurons were observed not only for axon-collaterals but for axo-dendritic and axo-axonal proximities as well. Obtaining simultaneous patch-clamp recordings of the respective pairs of neurons allowed for testing their functional synaptic connectivity. None of the spatial proximities observed translated into synaptic connectivity between the respective cells. Supplementary Figure 2 (Synopsis Figure 5) shows axo-axonal and axo-dendritic proximities not shown in the publication and provides a single-sweep resolution of the connectivity screening for the pair of STN neurons tested.

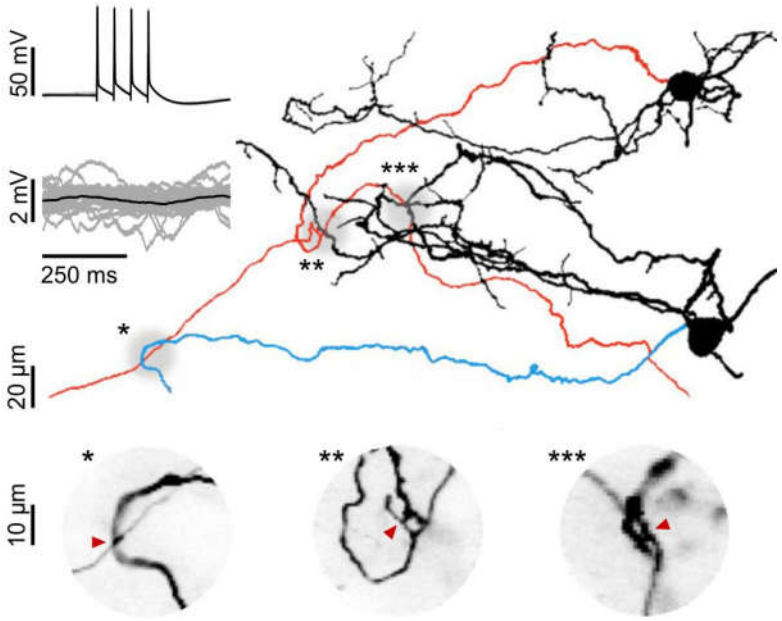

Synopsis Figure 5. Supplementary Figure 2 (linked to Figure 2B & 3 of Steiner et al., 2019).
2D representation of two reconstructed STN neurons with axo-axonic (*) and axo-dendritic (**,***) proximities. Somata and dendrites are depicted in black, axons are shown in red (putative presynaptic neuron) and blue (putative postsynaptic neuron). Gray circles highlight sites of proximity. Insets show confocal z-stack close-ups of the proximities. Red arrows point to potential contact site. Top left: Corresponding single sweep resolution of the tested pair of neurons. Upper traces show a train of four action potentials elicited in the putative presynaptic neuron. Lower traces show simultaneous recording of putative postsynaptic neuron (grey: single sweeps; black: 40 sweep average).

4.3 Supplementary Figure 3: The rat STN represents a vGAT-negative structure

The animals used in this study express Venus-YFP (yellow fluorescent protein) under the vGAT- (vesicular GABA transporter) promoter to allow for labeling of putative GABAergic neurons by means of probing vGAT-YFP fluorescence in epifluorescence illumination. The rat STN proved to be a vGAT-negative structure in both juvenile and adult animals (Synopsis Figure 6). While this finding does not unequivocally refute the existence of some GABAergic neurons in the rat STN, it makes the targeted recording of potential GABAergic cells impossible in this reporter line. On a more general note, no cells that were clearly identified as being within the STN were excluded in this study. Because of the many neurons recorded from, it can be assumed that neuronal subtypes, if present, are included in the examined sample and thus represented in the connectivity analysis.

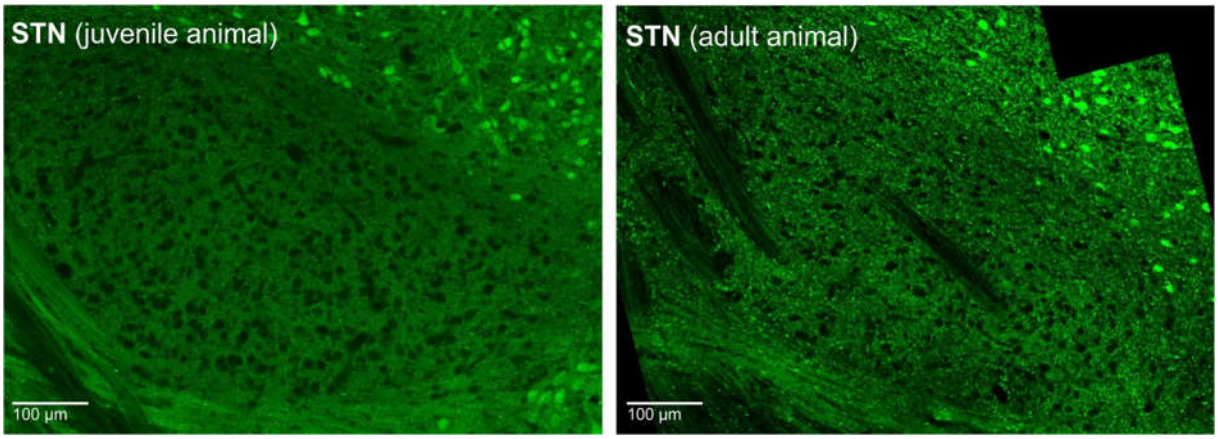

Synopsis Figure 6. Supplementary Figure 3 (linked to Figure 1D of Steiner et al., 2019).
Overview immunofluorescence images of the STN from vGAT-YFP transgenic rats. YFP-signal was enhanced via post-hoc YFP-antibody stainings. Left: animal from the juvenile cohort; right: animal from the adult cohort.

4.4 Supplementary Figure 4: Patterns of spontaneous activity observed in the sample of STN neurons examined

Most of the neurons examined did not exhibit spontaneous activity. This might be due to the whole cell approach used in this study. The whole cell approach was necessary to achieve fast access to the recorded cells and maintain stability of recordings to allow for multi-patch experiments.

Nevertheless, activity patterns of spontaneous activity were observed in a small subset of neurons: spontaneous bursting (Synopsis Figure 7A), tonic spontaneous activity (Synopsis Figure 7B) and plateau potentials (>200 ms) following hyperpolarizing pulses (Synopsis Figure 7C). Because of the recording condition chosen (see above), it is likely that occurrence of spontaneous activity in the examined sample of STN neurons is not representative and therefore best studied in future perforated-patch experiments.

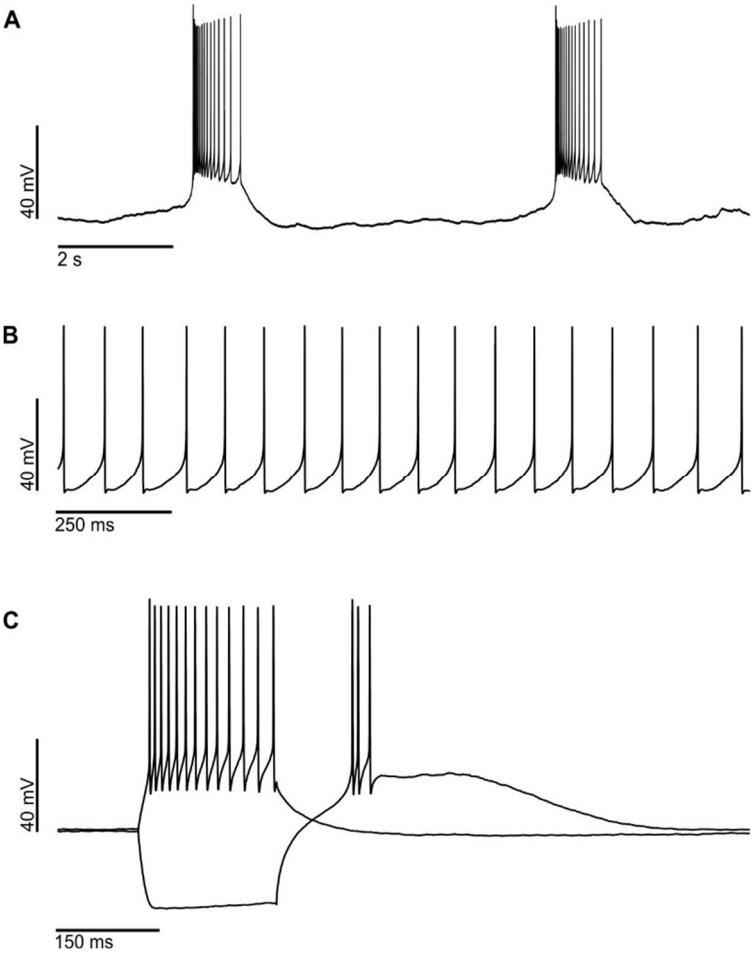

Synopsis Figure 7. Supplementary Figure 4 (linked to Figure 1C of Steiner et al., 2019).
Exemplary voltage traces of STN neurons. (A) Spontaneous bursting activity of an individual STN neurons. (B) Tonic spontaneous activity of another STN neuron. (C) STN neuron exhibiting a plateau potential with rebound action potential discharge following a hyperpolarizing pulse.

(5) DISCUSSION beyond the publication

5.1 The functional and structural organization of the STN microcircuitry

5.1.1 Functional synaptic wiring of the STN neurons

In the introduction to this thesis, it has been argued that *different patterns of intrinsic and afferent synaptic connectivity in the STN* are conceivable and need to be experimentally tested (Synopsis Figure 2). Referring back to these *proposed patterns that allow for neuronal synchrony in the STN,* the following summarizes related findings as provided in Steiner et al., 2019 (for illustration see Synopsis Figure 8):

Rejected hypothesis (A): Intranuclear mutual connectivity promotes the emergence of intrinsic synchrony.

No mutual synaptic connectivity between STN neurons was found despite the many connections tested (n=874). Therefore, mutual synaptic connectivity between STN neurons is improbable and not suited to explain the emergence of local synchrony (Synopsis Figure 8A).

Rejected hypothesis (B): Divergent connectivity of single afferent fibers causes the synchronous recruitment of STN neurons.

Combination of multi-patch recordings with a minimal stimulation protocol allowed for the testing of divergence of incoming projections which might serve for synchronous recruitment of STN neurons. The evidence provided by Steiner et al., 2019 makes this possibility improbable showing sparse and selective innervation patterns of single afferent fibers (Synopsis Figure 8B).

Approved hypotheses (C & D): Coordinated activity of presynaptic structures up-stream of the STN interacting with the STN via sparse and selective input.

Scenario A or B are improbable given the findings provided in Steiner et al., 2019. Hence, by means of hypotheses elimination, scenario C or D, which both rely on sparse and selective single fiber input to the STN, are most likely (Synopsis Figure 8 C & D). Indeed, interconnectivity of GPe neurons via local axon-collaterals has been confirmed by paired patch-clamp recordings (Bugaysen et al., 2013) and cortical pyramidal cells have been shown to be synchronized at beta frequencies by local interneurons (Lacey et al., 2014).

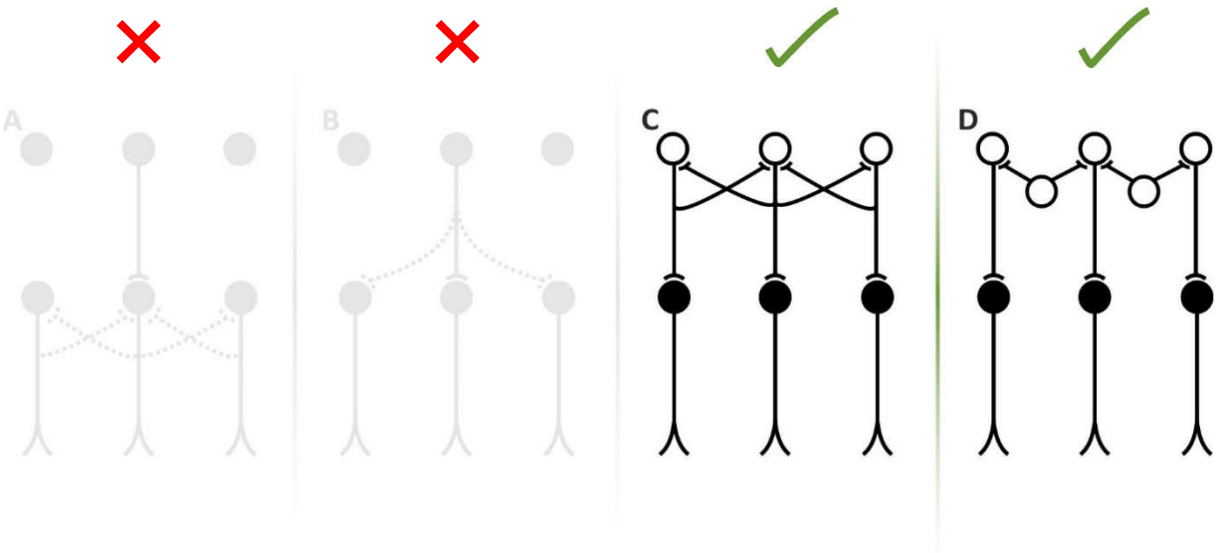

Synopsis Figure 8. Schemes illustrating results of intrinsic and afferent connectivity analysis (see text for descriptions and results of testing of rules). Empty circles represent somata of neurons afferent to the STN (e.g. Cortex or GPe). Filled circles represent somata of STN neurons. Red crosses indicate rejected hypotheses A and B; green arrows indicate approved hypotheses C and D.

In conclusion, neuronal synchronization dynamics that contribute to the physiology of the rat STN are likely to rely on sparse single fiber input rather than broad divergence of single afferent fibers or mutual connectivity between STN neurons. Together, this argues for STN neurons as being best conceived as parallel processing units. Thus, synchronization of firing patterns of local populations of STN neurons will require synchronized input.

5.1.2 Structural properties of STN afferents

As discussed above, synaptic control of STN synchrony can be expected to exclusively rely on STN afferents that comprise sparse and selective GABAergic and glutamatergic projections to the STN.

Previous anatomical work has suggested that single GABAergic fibers show sparse connectivity to local clusters of STN neurons (Baufreton et al., 2009). The experiments reported in Steiner et al., 2019 (Figure 4) support this hypothesis on a functional level. Importantly, Steiner et al., 2019 extends the analysis to glutamatergic fibers that display similar or even more selective innervation patterns than their GABAergic counterparts. Furthermore, structural differences between glutamatergic and GABAergic afferent fibers innervating the STN may be able to explain the differential dynamics of glutamatergic and GABAergic inputs during high-frequency stimulation (Figure 6, Steiner

et al., 2019). The following paragraphs will draw from the existing literature to probe such consistency.

Comparison of previous electron-microscopy work shows a considerable difference in the number of boutons of hyperdirect (4 - 94 glutamatergic boutons, rat (Kita and Kita, 2012)) and indirect (44 - 466 GABAergic boutons, rat (Kita and Kita, 2012)) fibers projecting to the rat STN. GABAergic terminals per single fiber do not only outnumber their glutamatergic counterparts, but individual terminals have also suggested to be larger (indirect GABAergic: 0,7 - 4,5 µm, rat (Smith et al., 1990) vs. hyperdirect glutamatergic: less than 1 µm, cat (Romansky et al., 1979) or 1,02 µm ± 0,06 µm (mean ± SEM), primate (Coude et al., 2018)). Furthermore, the single GABAergic axons connect to individual STN neurons by multiple synaptic contacts (Baufreton et al., 2009), adding to the relative potency of single GABAergic fiber innervation in comparison to glutamatergic fibers belonging to the hyperdirect pathway, that have been shown to form sparse terminal fields in the STN (Kita et al., 2012).

Together, this argues for larger pools of vesicles in GABAergic compared to glutamatergic single axon projections. This in turn can be expected to make GABAergic transmission less prone to synaptic depression as it has been shown that synaptic dynamics of short-term depression depend - among other factors - on vesicle reservoir and release dynamics (Zucker and Regehr, 2002). Hence, ultrastructural findings support the relative robustness of GABAergic transmission to HFS (Figure 6, Steiner et al., 2019).

5.2 Synaptic control of the STN and the DBS mechanism of action

5.2.1 DBS mediated control of neuronal synchrony in the STN

In a second set of experiments the unique opportunity of the multi-patch set-up was used to study alterations in afferent control of the STN in a DBS-like scenario.

DBS mechanisms of action have been under debate ever since its introduction into clinical practice in the 1980s. Early on, it has been suggested that DBS effects might be comparable to transient beneficial lesions of the stimulated structure (Benabid et al., 1987). While it has been confirmed that stimulation does suppress neuronal activity of STN neurons (Milosevic et al., 2019), it simultaneously recruits afferent and efferent fibers, resulting in ortho- and antidromic action potential (AP) propagation and thus wide-spread effects.

Steiner et al., 2019 suggests that sparse and selective afferents control STN neuronal synchrony and argues that DBS-like orthodromic stimulation of STN afferents is

responsible for the control of synchronization within the STN. This is not to say, however, that afferent antidromic or efferent effects of DBS do not contribute to its mechanism of action. All of these effects are likely to complement each other. Nonetheless, there is good reason to study the mechanisms that govern synchrony in the STN: Therapeutically effective DBS has been shown to decrease exaggerated synchrony in the STN (Kuhn et al., 2008) and STN synchrony has received attention as a biomarker for physiological processing (Mirzaei et al., 2017) and as a pathophysiological correlate of Parkinson's Disease (Tinkhauser et al., 2017a).

Previous work has stressed the importance of high temporal resolution in the control of STN synchrony via intermittent and feedback-controlled adaptive DBS (aDBS), that only applies stimulation when a defined threshold of synchrony is surpassed (Little et al., 2013). Importantly, STN synchrony is a dynamic feature of motor performance and fluctuates over time to give bursts of oscillatory activity. While short-lived bursts of synchrony in the beta frequency band have shown to be an important feature of physiological processing (Mirzaei et al., 2017), prolonged beta bursts are linked to motor impairment (Tinkhauser et al., 2017a). In order to retune dynamics of synchronization, aDBS therefore aims to truncate long beta bursts and thus exaggerated local synchronization in the STN. To do so, destruction of synchrony has to be achieved in the time course of milliseconds (Ramirez-Zamora et al., 2017). Only then, aDBS can comply with the temporal scale of synchronization dynamics and allow for physiological synchronization dynamics in inter-stimulation intervals. Steiner et al., 2019 argues that the short-term plasticity of glutamatergic and GABAergic inputs may provide a mechanistic explanation for such moment-to-moment control of STN synchrony. In short, findings provided in Steiner et al., 2019 suggest this may rely on the following:

- The particular susceptibility of the glutamatergic input to synaptic depression upon repetitive stimulation at high frequencies selectively decouples the STN from its synchronizing glutamatergic cortical drive within tens of milliseconds (Figure 6, Steiner et al., 2019; Synopsis Figure 9).
- The sustained inhibitory input will promote desynchronization as it directly shunts excitatory postsynaptic currents (Figure 5, Steiner et al., 2019) and may directly counteract disinhibition of the STN (a hallmark of PD pathophysiology).

- The synaptic recovery of depressed inputs is complete within seconds (Figure 6, Steiner et al., 2019), so that intermittent DBS may allow for physiological synchronization dynamics in inter-stimulation intervals.

The aforementioned effects cumulate in a temporally restricted synaptic decoupling of the STN from synchronizing afferent control and are thus in good agreement with the temporal precision needed in intermittent stimulation paradigms such as aDBS.

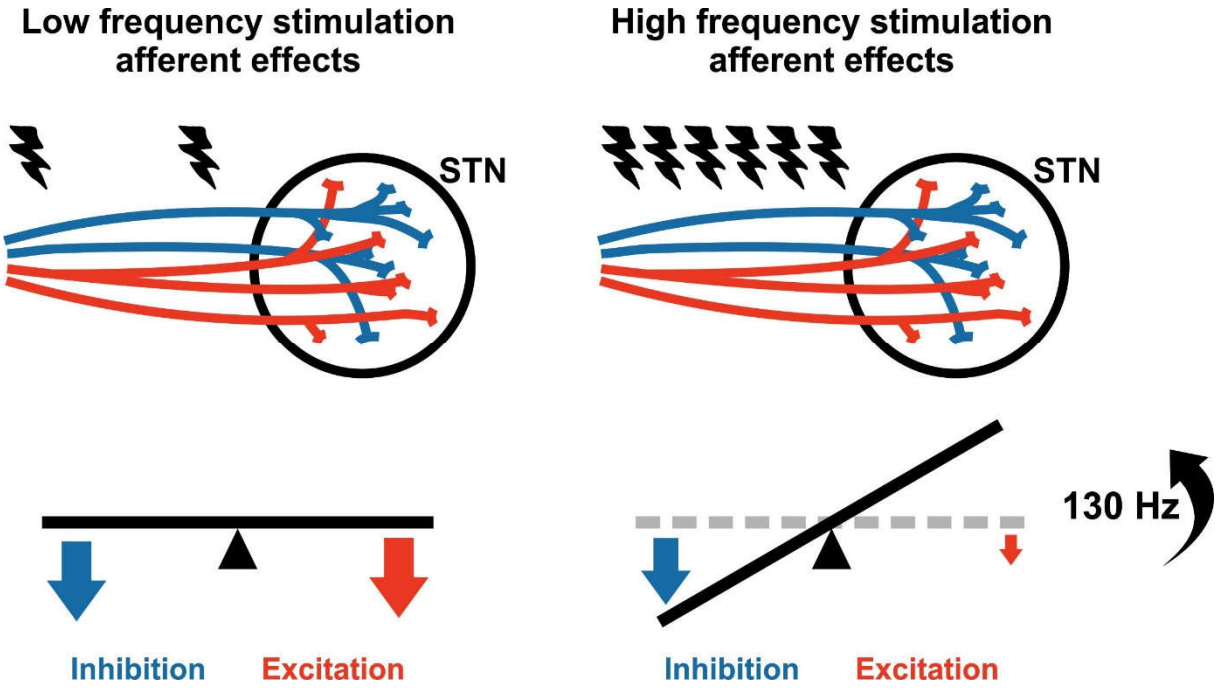

Synopsis Figure 9. High-frequency stimulation of the STN results in a shift towards inhibition. Upper panels: Illustration of low and high frequency activation of STN afferents. Red lines represent glutamatergic fibers; blue lines represent GABAergic fibers. Flashes visualize extracellular electric stimulation. Lower panels: Effects of low vs. high frequency extracellular stimulation on the balance between synaptic inhibition (illustrated by blue arrows) and excitation (illustrated by red arrows) in the STN as suggested by Figure 6, Steiner et al., 2019. Note that during low frequency stimulation, synaptic inhibition and excitation were depressed to similar degrees. During high frequency stimulation, however, depression of excitatory input was almost complete after only five stimuli in contrast to GABAergic transmission that proved to be relatively robust to high frequency stimulation. In consequence, high-frequency stimulation (130 Hz) of the STN can be expected to result in a shift towards synaptic inhibition.

5.2.3 Synaptic inhibition in the STN – a double-edged sword

The indirect pathway has been assigned an important role in the parkinsonian pathophysiology. Previous work has suggested an amplified synaptic strength of the GPe–STN projection in the dopamine depleted state (Fan et al., 2012). Importantly, enhanced GABAergic transmission at the level of STN inputs can translate into augmented synchronization of neuronal activity by increasing the availability of Na^+ channels (Baufreton et al., 2005). At first sight, this synchrony promoting role of

GABAergic inputs to the STN might contradict what has been argued above, namely, that stimulation of STN afferents at high frequencies results in a shift to GABAergic transmission that may be therapeutic. To dissolve the paradoxon of a both pathological and therapeutic role of synaptic inhibition in the STN, the contribution of phase relationships of synaptic input to neuronal synchrony in the STN has to be considered. It has been shown that synaptic excitation and inhibition to the STN settle in an anti-phasic relationship in the dopamine-depleted state (Mallet et al., 2008). The longer this phase relationship is maintained, the stronger the synchronization of neuronal activity in the STN (Cagnan et al., 2015). Steiner et al., 2019 argues that DBS actively shunts synaptic excitation and inhibition, inverting the synchronizing role of GABAergic signaling by *in phase stimulation* (Figure 5, Steiner et al., 2019). Specifically, desynchronization of AP generation by simultaneous activation of GABAergic and glutamatergic synaptic input proved to depend on GABAergic inputs, as glutamatergic input in isolation recruited STN neurons with high synchrony. Thus, enhanced GABAergic inhibition in the parkinsonian context may indeed serve DBS to more effectively interfere with pathologically rigid phase relationships, unlocking the circuit from synchrony promoting conditions.

Steiner et al., 2019 (Figure 5) not only provides evidence that *in phase* activation of GABAergic input has a desynchronizing effect but also shows how GABAergic co-stimulation serves to delay AP generation in STN neurons to >20 ms after the stimulation pulse (median: 20.2 ms, interquartile range 6.81–119.8 ms, n=32), compared to <8 ms AP latency when elicited by glutamatergic inputs in isolation (median: 7.3 ms, interquartile range 4.53 to 8.6, n=22). If stimulation is applied at 130 Hz, intervals between individual stimuli are <8 ms. Because the delay of AP generation resulting from repeatedly activated GABAergic afferents exceeds this interval between stimuli, it may effectively contribute to the suppression of firing rates of STN neurons that has been observed during high frequency stimulation of the STN (Milosevic et al., 2019).

In conclusion, differential short-term depression of STN inputs at high stimulation frequencies arguably represents a mechanism to both cause a timely precise deconstruction of STN synchrony and a suppression of STN firing rates, pointing to a dual therapeutic role of sustained and repeatedly activated synaptic inhibition.

5.2.3 Relations to previously described DBS mechanisms of action

It has been proposed that DBS dissociates inputs and outputs of its target structures, thereby interfering with pathological signaling (Nambu and Tachibana, 2014; Rosenbaum

et al., 2014). Previous work suggests this might be achieved by blocking trans-subthalamic loops (hyperdirect and indirect) at the level of the STN, sparring the disruption of other pathways (Maurice et al., 2003).

Previous work in acute brain slices has suggested that blocking incoming and outgoing neuronal communication might be achieved by means of conduction block of both STN afferent and efferent axons (Zheng et al., 2011). The authors report that HFS results in a reduction of fiber volley amplitude, a measure of the number of activated axons. Drawing from data collected at Substantia Nigra pars reticulata (SNr) afferent synapses, Rosenbaum et al. developed a computational model of axonal and synaptic failure aiming to simulate dynamics of DBS-induced short-term depression (Rosenbaum et al., 2014). Due to distinct properties of the respective axons (see section 5.1.2), disruption of axonal conduction within the STN might differ between glutamatergic and GABAergic fibers. Thus, it would be conceivable to explain differential short-term synaptic dynamics by means of differential probabilities for axonal failure. However, Zheng et al. report a striking difference in the time scale of HFS-induced axonal (decay time constant of fiber volley amplitudes at SNr afferent synapses*:* 1.57 ± 0.11 s (mean ± SEM; n=7)) and much faster synaptic failure (decay time constant of EPSCs at SNr afferent synapses*:* 0.1 ± 0.02 s (mean ± SEM; n=5)) and conclude that axonal failure might contribute to but cannot fully explain the much faster decline in postsynaptic currents. Data provided in Steiner et al., 2019 suggests that attenuation of afferent glutamatergic input to the STN is achieved within <50 ms (Figure 6, Steiner et al., 2019) and thus even faster than the decline of synaptic amplitudes Zheng et al. have reported for SNr input synapses. For these reasons, axonal failure might contribute to the mechanism of action of continuous DBS, but is insufficient to explain how intermittent stimulation paradigms interact with oscillatory activity in a sub-second timeframe.

In their review from 2014, Nambu and Tachibana discuss other possible mechanisms of DBS-induced STN decoupling (Nambu and Tachibana, 2014). They suggest an equivalency of STN DBS (Maurice et al., 2003) and GABA-A-Agonist (muscimol) injection into the STN (Nambu et al., 2000), as both result in similar circuit dynamics reminiscent of a selective disruption of trans-subthalamic pathways. Nambu and Tachibana speculate that this equivalence may be achieved by stimulation of GABAergic fibers. Indeed, there is evidence that focal release of GABA at afferent terminals in the STN may be therapeutically effective in humans (Levy et al., 2001). However, electrical stimulation activates not only GABAergic, but glutamatergic axons alike. While Nambu and

Tachibana conclude that the composition of stimulated fibers may determine the DBS effect, data provided in Steiner et al., 2019 offer an alternative explanation. The proposed equivalency may be directly explained by differential short-term depression of synaptic inputs to the STN: High-frequency stimulation of STN will not only decouple the STN from hyperdirect excitation, but the lasting release of GABA may have an analogous effect to artificial GABA-A-receptor-agonist (muscimol) injections into the STN.

Finally, it has been shown that exaggerated synchrony in the STN can be counteracted by local micro-injections of glutamate-receptor antagonists (CPP and NBQX; (Tachibana et al., 2011)). Pharmacological suppression of glutamatergic signaling can be expected to have an analogous effect to the almost complete suppression of EPSCs during HFS (Figure 6, Steiner et al., 2019). Thus, findings provided in Steiner et al., 2019 integrate evidence suggesting that the DBS mechanism of action depends on the release of GABA with other studies that have shown that the high frequency stimulation of the hyperdirect pathway is effective in itself (Sanders and Jaeger, 2016).

5.3 Conclusion

In conclusion, the in vitro multi-patch approach used in Steiner et al., 2019 has provided the opportunity to study both the intrinsic and afferent synaptic connectivity of the STN. This allowed for the characterization of STN neurons as parallel processing units that need to be synchronized by afferent structures interacting with the STN via sparse and selective single fiber innervation.

Combination of the multi-patch paradigm with frequency-varied extracellular stimulation has shed light on the contribution of glutamatergic and GABAergic input to synaptic control of STN synchrony. The reported differential short-term depression of these inputs during high frequency stimulation may provide a synaptic mechanism to reconcile and integrate previously described DBS mechanisms of action.

Together, the findings of this dissertation provide constraints for future, more realistic computational models of the basal ganglia circuitry and will deepen the understanding of how next-generation DBS applications may allow for moment-to-moment control of STN synchrony.

(6) REFERENCES

Baufreton J, Atherton JF, Surmeier DJ, Bevan MD (2005) Enhancement of excitatory synaptic integration by GABAergic inhibition in the subthalamic nucleus. J Neurosci 25:8505-8517.

Baufreton J, Kirkham E, Atherton JF, Menard A, Magill PJ, Bolam JP, Bevan MD (2009) Sparse but selective and potent synaptic transmission from the globus pallidus to the subthalamic nucleus. J Neurophysiol 102:532-545.

Benabid AL, Pollak P, Louveau A, Henry S, de Rougemont J (1987) Combined (thalamotomy and stimulation) stereotactic surgery of the VIM thalamic nucleus for bilateral Parkinson disease. Appl Neurophysiol 50:344-346.

Bugaysen J, Bar-Gad I, Korngreen A (2013) Continuous modulation of action potential firing by a unitary GABAergic connection in the globus pallidus in vitro. J Neurosci 33:12805-12809.

Cagnan H, Duff EP, Brown P (2015) The relative phases of basal ganglia activities dynamically shape effective connectivity in Parkinson's disease. Brain 138:1667-1678.

Coude D, Parent A, Parent M (2018) Single-axon tracing of the corticosubthalamic hyperdirect pathway in primates. Brain Struct Funct 223:3959-3973.

Fan KY, Baufreton J, Surmeier DJ, Chan CS, Bevan MD (2012) Proliferation of external globus pallidus-subthalamic nucleus synapses following degeneration of midbrain dopamine neurons. J Neurosci 32:13718-13728.

Geiger JR, Lubke J, Roth A, Frotscher M, Jonas P (1997) Submillisecond AMPA receptor-mediated signaling at a principal neuron-interneuron synapse. Neuron 18:1009-1023.

Gillies A, Willshaw D (2004) Models of the subthalamic nucleus. The importance of intranuclear connectivity. Med Eng Phys 26:723-732.

Hammond C, Yelnik J (1983) Intracellular labelling of rat subthalamic neurones with horseradish peroxidase: computer analysis of dendrites and characterization of axon arborization. Neuroscience 8:781-790.

Kita H, Chang HT, Kitai ST (1983) The morphology of intracellularly labeled rat subthalamic neurons: a light microscopic analysis. J Comp Neurol 215:245-257.

Kita T, Kita H (2012) The subthalamic nucleus is one of multiple innervation sites for long-range corticofugal axons: a single-axon tracing study in the rat. J Neurosci 32:5990-5999.

Koshimizu Y, Fujiyama F, Nakamura KC, Furuta T, Kaneko T (2013) Quantitative analysis of axon bouton distribution of subthalamic nucleus neurons in the rat by single neuron visualization with a viral vector. J Comp Neurol 521:2125-2146.

Kuhn AA, Kempf F, Brucke C, Gaynor Doyle L, Martinez-Torres I, Pogosyan A, Trottenberg T, Kupsch A, Schneider GH, Hariz MI, Vandenberghe W, Nuttin B, Brown P (2008) High-frequency stimulation of the subthalamic nucleus suppresses oscillatory beta activity in patients with Parkinson's disease in parallel with improvement in motor performance. J Neurosci 28:6165-6173.

Lacey MG, Gooding-Williams G, Prokic EJ, Yamawaki N, Hall SD, Stanford IM, Woodhall GL (2014) Spike firing and IPSPs in layer V pyramidal neurons during beta oscillations in rat primary motor cortex (M1) in vitro. PLoS One 9:e85109.

Levy R, Lang AE, Dostrovsky JO, Pahapill P, Romas J, Saint-Cyr J, Hutchison WD, Lozano AM (2001) Lidocaine and muscimol microinjections in subthalamic nucleus reverse Parkinsonian symptoms. Brain 124:2105-2118.

Little S, Pogosyan A, Neal S, Zavala B, Zrinzo L, Hariz M, Foltynie T, Limousin P, Ashkan K, FitzGerald J, Green AL, Aziz TZ, Brown P (2013) Adaptive deep brain stimulation in advanced Parkinson disease. Ann Neurol 74:449-457.

Mallet N, Pogosyan A, Marton LF, Bolam JP, Brown P, Magill PJ (2008) Parkinsonian beta oscillations in the external globus pallidus and their relationship with subthalamic nucleus activity. J Neurosci 28:14245-14258.

Maurice N, Thierry AM, Glowinski J, Deniau JM (2003) Spontaneous and evoked activity of substantia nigra pars reticulata neurons during high-frequency stimulation of the subthalamic nucleus. J Neurosci 23:9929-9936.

Milosevic L, Kalia SK, Hodaie M, Lozano A, Popovic MR, Hutchison W (2019) Subthalamic suppression defines therapeutic threshold of deep brain stimulation in Parkinson's disease. J Neurol Neurosurg Psychiatry 90:1105-1108.

Mirzaei A, Kumar A, Leventhal D, Mallet N, Aertsen A, Berke J, Schmidt R (2017) Sensorimotor Processing in the Basal Ganglia Leads to Transient Beta Oscillations during Behavior. J Neurosci 37:11220-11232.

Nambu A, Tachibana Y (2014) Mechanism of parkinsonian neuronal oscillations in the primate basal ganglia: some considerations based on our recent work. Front Syst Neurosci 8:74.

Nambu A, Tokuno H, Takada M (2002) Functional significance of the cortico-subthalamo-pallidal 'hyperdirect' pathway. Neurosci Res 43:111-117.

Nambu A, Tokuno H, Hamada I, Kita H, Imanishi M, Akazawa T, Ikeuchi Y, Hasegawa N (2000) Excitatory cortical inputs to pallidal neurons via the subthalamic nucleus in the monkey. J Neurophysiol 84:289-300.

Peng Y, Mittermaier FX, Planert H, Schneider UC, Alle H, Geiger JR (2019) High-throughput microcircuit analysis of individual human brains through next-generation multineuron patch-clamp. Elife 8.

Ramirez-Zamora A et al. (2017) Evolving Applications, Technological Challenges and Future Opportunities in Neuromodulation: Proceedings of the Fifth Annual Deep Brain Stimulation Think Tank. Front Neurosci 11:734.

Romansky KV, Usunoff KG, Ivanov DP, Galabov GP (1979) Corticosubthalamic projection in the cat: an electron microscopic study. Brain Res 163:319-322.

Rosenbaum R, Zimnik A, Zheng F, Turner RS, Alzheimer C, Doiron B, Rubin JE (2014) Axonal and synaptic failure suppress the transfer of firing rate oscillations, synchrony and information during high frequency deep brain stimulation. Neurobiol Dis 62:86-99.

Sanders TH, Jaeger D (2016) Optogenetic stimulation of cortico-subthalamic projections is sufficient to ameliorate bradykinesia in 6-ohda lesioned mice. Neurobiol Dis 95:225-237.

Shen KZ, Johnson SW (2006) Subthalamic stimulation evokes complex EPSCs in the rat substantia nigra pars reticulata in vitro. J Physiol 573:697-709.

Smith Y, Bolam JP, Von Krosigk M (1990) Topographical and Synaptic Organization of the GABA-Containing Pallidosubthalamic Projection in the Rat. Eur J Neurosci 2:500-511.

Steiner LA, Barreda Tomas FJ, Planert H, Alle H, Vida I, Geiger JRP (2019) Connectivity and Dynamics Underlying Synaptic Control of the Subthalamic Nucleus. J Neurosci 39:2470-2481.

Tachibana Y, Iwamuro H, Kita H, Takada M, Nambu A (2011) Subthalamo-pallidal interactions underlying parkinsonian neuronal oscillations in the primate basal ganglia. Eur J Neurosci 34:1470-1484.

Tinkhauser G, Pogosyan A, Tan H, Herz DM, Kuhn AA, Brown P (2017a) Beta burst dynamics in Parkinson's disease OFF and ON dopaminergic medication. Brain 140:2968-2981.

Tinkhauser G, Pogosyan A, Little S, Beudel M, Herz DM, Tan H, Brown P (2017b) The modulatory effect of adaptive deep brain stimulation on beta bursts in Parkinson's disease. Brain 140:1053-1067.

Wilson CL, Puntis M, Lacey MG (2004) Overwhelmingly asynchronous firing of rat subthalamic nucleus neurones in brain slices provides little evidence for intrinsic interconnectivity. Neuroscience 123:187-200.

Zheng F, Lammert K, Nixdorf-Bergweiler BE, Steigerwald F, Volkmann J, Alzheimer C (2011) Axonal failure during high frequency stimulation of rat subthalamic nucleus. J Physiol 589:2781-2793.

Zucker RS, Regehr WG (2002) Short-term synaptic plasticity. Annu Rev Physiol 64:355-405.

(7) AFFIDAVID

7.1 Statutory declaration

"I, Leon Amadeus Steiner, by personally signing this document in lieu of an oath, hereby affirm that I prepared the submitted dissertation on the topic Connectivity and Dynamics Underlying Synaptic Control of the Subthalamic Nucleus (German: Konnektivität und Dynamik der Synaptischen Kontrolle des Nucleus Subthalamicus) independently and without the support of third parties, and that I used no other sources and aids than those stated.

All parts which are based on the publications or presentations of other authors, either in letter or in spirit, are specified as such in accordance with the citing guidelines. The sections on methodology (in particular regarding practical work, laboratory regulations, statistical processing) and results (in particular regarding figures, charts and tables) are exclusively my responsibility.

Furthermore, I declare that I have correctly marked all of the data, the analyses, and the conclusions generated from data obtained in collaboration with other persons, and that I have correctly marked my own contribution and the contributions of other persons (cf. declaration of contribution). I have correctly marked all texts or parts of texts that were generated in collaboration with other persons.

My contributions to the publication to this dissertation correspond to those stated in the below joint declaration made together with the supervisor. The publication created within the scope of the dissertation complies with the guidelines of the ICMJE (International Committee of Medical Journal Editors; www.icmje.org) on authorship. In addition, I declare that I shall comply with the regulations of Charité – Universitätsmedizin Berlin on ensuring good scientific practice.

I declare that I have not yet submitted this dissertation in identical or similar form to another Faculty.

The significance of this statutory declaration and the consequences of a false statutory declaration under criminal law (Sections 156, 161 of the German Criminal Code) are known to me."

MD/PhD – candidate

7.2 Detailed declaration of contribution to the publication

Leon Amadeus Steiner contributed the following to the below listed publication:

Publication:
Steiner L.A., Barreda Tomas F.J., Planert H., Alle H., Vida I., Geiger J.R.P., Connectivity and Dynamics Underlying Synaptic Control of the Subthalamic Nucleus, Journal of Neuroscience, 2019.

Contribution in detail**:**

Conception:

This study was conceptualized by Prof. Dr. Jörg Geiger, PD Dr. Henrik Alle and Leon Amadeus Steiner.

Methods:

Leon Amadeus Steiner optimized the experimental set-up featuring eight micromanipulators to meet requirements of the experimental paradigm used. This involved custom hardware solutions to allow for the combination of multiple simultaneous recordings and extracellular stimulation. Leon Amadeus Steiner performed all lab work required for the experimental procedures including fabrication and optimization of artificial cerebral spinal fluids and artificial intracellular solutions, preparations of rat brains and subsequent slicing (with exception of the control experiments in the adult rat cohort. In addition, Leon Amadeus Steiner performed the initial stages of the neuroanatomical staining (with exception of the control experiments in the adult rat cohort).

Experiments:

Leon Amadeus Steiner performed all electrophysiological experiments (with exception of the control experiments in the adult rat cohort).

Analysis, Visualization & Manuscript:

All electrophysiological data (with exception of the control experiments in the adult rat cohort) were analyzed by Leon Amadeus Steiner. Leon Amadeus Steiner wrote the first draft of the paper (with exception of the paragraphs referring to neuroanatomical results), created all schematic illustrations and all figures that display electrophysiological data (Figure 1 A-C, Figure 2 B and C, Figure 4, Figure 5 and Figure 6, Steiner et al., 2019).

Neuroanatomical figures (Figure 1 D and E, Figure 2 A, Figure 3, Steiner et al., 2019) were created by Federico J. Barreda Tomas in close collaboration with Leon Amadeus Steiner. All co-authors contributed to the manuscript, the figures and the review process through comments and suggestions.

MD/PhD – supervisor

MD/PhD – candidate

(8) EXCERPT FROM THE ISI JOURNAL SUMMARY LIST

Journal Data Filtered By: **Selected JCR Year: 2017** Selected Editions: SCIE,SSCI
Selected Categories: **"NEUROSCIENCES"** Selected Category Scheme: WoS
Gesamtanzahl: 261 Journale

Rank	Full Journal Title	Total Cites	Journal Impact Factor	Eigenfactor Score
1	NATURE REVIEWS NEUROSCIENCE	40,834	32.635	0.069940
2	NATURE NEUROSCIENCE	59,426	19.912	0.153710
3	ACTA NEUROPATHOLOGICA	18,783	15.872	0.041490
4	TRENDS IN COGNITIVE SCIENCES	25,391	15.557	0.040790
5	BEHAVIORAL AND BRAIN SCIENCES	8,900	15.071	0.010130
6	Annual Review of Neuroscience	13,320	14.675	0.016110
7	NEURON	89,410	14.318	0.216730
8	PROGRESS IN NEUROBIOLOGY	13,065	14.163	0.015550
9	BIOLOGICAL PSYCHIATRY	42,494	11.982	0.056910
10	MOLECULAR PSYCHIATRY	18,460	11.640	0.047200
11	JOURNAL OF PINEAL RESEARCH	9,079	11.613	0.008600
12	TRENDS IN NEUROSCIENCES	20,061	11.439	0.026860
13	BRAIN	52,061	10.840	0.075170
14	SLEEP MEDICINE REVIEWS	6,080	10.602	0.010720
15	ANNALS OF NEUROLOGY	37,251	10.244	0.053390
16	Translational Stroke Research	2,202	8.266	0.005260
17	NEUROSCIENCE AND BIOBEHAVIORAL REVIEWS	24,279	8.037	0.048460
18	NEUROSCIENTIST	4,738	7.461	0.008730
19	NEURAL NETWORKS	10,086	7.197	0.015290
20	FRONTIERS IN NEUROENDOCRINOLOGY	3,924	6.875	0.006040
21	NEUROPSYCHOPHARMACOLOGY	24,537	6.544	0.042870
22	CURRENT OPINION IN NEUROBIOLOGY	14,190	6.541	0.034670
23	Molecular Neurodegeneration	3,489	6.426	0.009850
24	CEREBRAL CORTEX	29,570	6.308	0.058970
25	BRAIN BEHAVIOR AND IMMUNITY	12,583	6.306	0.026850
26	BRAIN PATHOLOGY	4,952	6.187	0.007750
27	Brain Stimulation	4,263	6.120	0.014510
28	NEUROPATHOLOGY AND APPLIED NEUROBIOLOGY	3,654	6.059	0.006350
29	JOURNAL OF CEREBRAL BLOOD FLOW AND METABOLISM	19,450	6.045	0.028280
30	JOURNAL OF NEUROSCIENCE	176,157	5.970	0.265950
31	Molecular Autism	1,679	5.872	0.006320
31	Translational Neurodegeneration	589	5.872	0.002280
33	GLIA	13,417	5.846	0.020530
34	Neurotherapeutics	3,973	5.719	0.008980
35	PAIN	36,132	5.559	0.038000
36	NEUROIMAGE	92,719	5.426	0.152610
37	Acta Neuropathologica Communications	2,326	5.414	0.011550
38	Multiple Sclerosis Journal	10,675	5.280	0.021890

(9) PUBLICATION

Title:

Connectivity and Dynamics Underlying Synaptic Control of the Subthalamic Nucleus

Authors:

Leon Amadeus Steiner, Federico J. Barreda Tomás, Henrike Planert, Henrik Alle, Imre Vida und Jörg R.P. Geiger

Journal:

Journal of Neuroscience

Date of publication:

Online publication ahead of print: 30.01.2019

Published in print: 27.03.2019

Systems/Circuits

Connectivity and Dynamics Underlying Synaptic Control of the Subthalamic Nucleus

Leon Amadeus Steiner,[1] Federico J. Barreda Tomás,[2] Henrike Planert,[1] Henrik Alle,[1] Imre Vida,[2,3] and Jörg R.P. Geiger[1,3]

[1]Institute of Neurophysiology, Charité-Universitätsmedizin Berlin, 10117 Berlin, Germany, [2]Institute of Integrative Neuroanatomy, Charité-Universitätsmedizin Berlin, 10117 Berlin, Germany, and [3]NeuroCure Cluster of Excellence, Charité-Universitätsmedizin Berlin, 10117 Berlin, Germany

Adaptive motor control critically depends on the interconnected nuclei of the basal ganglia in the CNS. A pivotal element of the basal ganglia is the subthalamic nucleus (STN), which serves as a therapeutic target for deep brain stimulation (DBS) in movement disorders, such as Parkinson's disease. The functional connectivity of the STN at the microcircuit level, however, still requires rigorous investigation. Here we combine multiple simultaneous whole-cell recordings with extracellular stimulation and *post hoc* neuroanatomical analysis to investigate intrinsic and afferent connectivity and synaptic properties of the STN in acute brain slices obtained from rats of both sexes. Our data reveal an absence of intrinsic connectivity and an afferent innervation with low divergence, suggesting that STN neurons operate as independent processing elements driven by upstream structures. Hence, synchrony in the STN, a hallmark of motor processing, exclusively depends on the interactions and dynamics of GABAergic and glutamatergic afferents. Importantly, these inputs are subject to differential short-term depression when stimulated at high, DBS-like frequencies, shifting the balance of excitation and inhibition toward inhibition. Thus, we present a mechanism for fast yet transient decoupling of the STN from synchronizing afferent control. Together, our study provides new insights into the microcircuit organization of the STN by identifying its neurons as parallel processing units and thus sets new constraints for future computational models of the basal ganglia. The observed differential short-term plasticity of afferent inputs further offers a basis to better understand and optimize DBS algorithms.

Key words: high-frequency stimulation; minimal stimulation; multipatch recordings; short-term plasticity; subthalamic nucleus; synaptic connectivity

Significance Statement

The subthalamic nucleus (STN) is a pivotal element of the basal ganglia and serves as target for deep brain stimulation, but information on the functional connectivity of its neurons is limited. To investigate the STN microcircuitry, we combined multiple simultaneous patch-clamp recordings and neuroanatomical analysis. Our results provide new insights into the synaptic organization of the STN identifying its neurons as parallel processing units and thus set new constraints for future computational models of the basal ganglia. We further find that synaptic dynamics of afferent inputs result in a rapid yet transient decoupling of the STN when stimulated at high frequencies. These results offer a better understanding of deep brain stimulation mechanisms, promoting the development of optimized algorithms.

Introduction

Adaptive motor control in vertebrates relies on the integrative properties of interconnected neuronal networks, including the motor cortex and the structures of the basal ganglia (Stephenson-Jones et al., 2011). Among the latter, the subthalamic nucleus (STN) is the only glutamatergic nucleus (Bolam et al., 2000). Further, it occupies a pivotal position within these circuits: it integrates complex afferent input, most prominently the cortical

Received June 29, 2018; revised Dec. 29, 2018; accepted Jan. 24, 2019.

Author contributions: L.A.S., F.J.B.T., H.A., I.V., and J.R.P.G. designed research; L.A.S., F.J.B.T., and H.P. performed research; L.A.S., F.J.B.T., and H.P. analyzed data; L.A.S. and F.J.B.T. wrote the first draft of the paper; L.A.S., F.J.B.T., H.P., H.A., I.V., and J.R.P.G. edited and wrote the paper.

This work was supported by German Research Foundation Grant KFO 247, the Cluster of Excellence NeuroCure EXC 257, and the Research Training Group GRK 1589. We thank Yangfan Peng for the design of the multiple patch-clamp recording setup and initial training; Ina Wolter for technical support with the immunocytochemical and histological processing; and Andrew Sharott, Wolf-Julian Neumann and Michael Daniel Hadler for helpful comments on an earlier version of the manuscript. VGAT-Venus transgenic rats were generated by Drs. Y. Yanagawa, M. Hirabayashi, and Y. Kawaguchi (National Institute for Physiological Sciences, Okazaki, Japan), using pCS2-Venus provided by Dr. A. Miyawaki.

The authors declare no competing financial interests.

Correspondence should be addressed to Jörg R.P. Geiger at joerg.geiger@charite.de.

https://doi.org/10.1523/JNEUROSCI.1642-18.2019

 0270-6474/19/392470-12$15.00/0

"hyperdirect" (Nambu et al., 2002) and the pallidal "indirect" pathway (Smith et al., 1990), and targets the main output nuclei of the basal ganglia. The STN has also received substantial attention as a major target for deep brain stimulation (DBS) to treat symptoms of Parkinson's disease (PD) (Benabid et al., 1994; Chen et al., 2006). Despite increasing interest in the physiology of the STN and its clinical relevance, however, intrinsic and afferent connectivity of STN neurons and their synaptic properties are not fully explored.

Under physiological conditions, neurons in the basal ganglia engage in brief transient synchronization at beta frequencies, and the dynamics of synchronization are instrumental to basal ganglia function (Feingold et al., 2015; Mirzaei et al., 2017; Tinkhauser et al., 2017a). Conversely, beta activity recorded in the STN is exaggerated in PD (Neumann et al., 2016; Steiner et al., 2017; Tinkhauser et al., 2017a), and clinically effective DBS reduces synchrony in this nucleus (Kühn et al., 2008). Nevertheless, little is known of the anatomical substrate underlying synchronization in the STN. As neuronal network synchrony may depend on both afferent and intrinsic connectivity, prime candidates, which could mediate synaptic control of neuronal synchrony in the STN, include the following: (1) glutamatergic afferents of the hyperdirect cortical input, (2) GABAergic afferents belonging to the indirect pathway, and (3) intranuclear mutual connectivity of STN neurons. In terms of afferent connectivity, there is limited information on the organization of incoming GABAergic inputs (Baufreton et al., 2009); however, functional connectivity of glutamatergic projections, potentially more critical to the control of synchrony in the STN (Gradinaru et al., 2009; Li et al., 2012; Sanders and Jaeger, 2016), is not well understood. More specifically, incoming fibers of both indirect (Baufreton et al., 2009) and hyperdirect pathways collateralize in the STN (Kita and Kita, 2012), and their divergence may serve as an anatomical prerequisite for synchronous recruitment. Mutual synaptic connectivity between STN neurons has been suggested on the basis of anatomical (Hammond and Yelnik, 1983; Kita et al., 1983; Chang et al., 1984; Ammari et al., 2010; Gouty-Colomer et al., 2018) and indirect electrophysiological observations (Shen and Johnson, 2006; Ammari et al., 2010; Chu et al., 2012), but these observations were called into question by contrasting findings (Wilson et al., 2004; Koshimizu et al., 2013). Thus, the mere existence of functional intranuclear connections remains contentious.

In the present study, we combine simultaneous whole-cell recordings of up to 7 neurons with extracellular stimulation and morphological analysis of the recorded neuronal clusters, to investigate the intrinsic and afferent functional connectivity of rat STN neurons. We further analyze functional properties and interactions of synaptic inputs to these neurons. Finally, we compare synaptic dynamics of both glutamatergic and GABAergic inputs in response to repetitive stimulation at low and high, DBS-like frequencies.

Materials and Methods

Slice preparation. Acute brain slices ($n = 64$) were prepared from 38 juvenile (P14-P21) transgenic Wistar rats of both sexes expressing Venus-YFP under the VGAT promoter (Uematsu et al., 2008) (RRID: RGD_2314361). To control for age-dependent effects, we performed additional experiments in a set of 4 adult animals (P61-P70). Animal handling and all procedures were performed in accordance with guidelines of local authorities (Berlin, [T0109/10]), the German Animal Welfare Act, and the European Council Directive 86/609/EEC. Animals were decapitated after receiving isoflurane anesthesia, and the head was immediately submerged in an ice-cold sucrose-based slicing solution containing the following (in mM): 196 sucrose, 2.5 KCl, 1.2 NaH_2PO_4, 20 glucose, 26 $NaHCO_3$, 0.5 $CaCl_2$, 3.5 $MgCl_2$ enriched with carbogen (95% O_2/5% CO_2).

Horizontal and parasagittal 300-μm-thick slices containing the STN were cut using a VT1200 vibratome (Leica Microsystems). Acute slices of both horizontal and parasagittal orientation were cut to enable comparison of our results with those of previous studies working in either of these two planes. Subsequently, slices were stored in an ACSF containing the following (in mM): 126 NaCl, 2.5 KCl, 1.2 NaH_2PO_4, 11 glucose, 19 $NaHCO_3$, 2.4 $CaCl_2$, 1.2 $MgCl_2$, bubbled with carbogen (95% O_2/5% CO_2). For recovery, slices were kept at 34°C for a minimum of 30 min. Slices were stored in an interface-type chamber in carbogenated ACSF for up to 5 h before being transferred to the recording chamber.

Whole-cell patch-clamp recordings. Recordings were performed in a submerged-type recording chamber continuously perfused with ACSF held at 34°C. Somatic whole-cell patch-clamp recordings were performed using pipettes pulled from borosilicate glass capillaries (2 mm outer/1 mm inner diameter) on a horizontal puller (P-97, Sutter Instrument). The pipettes were filled with an intracellular solution containing the following (in mM): 145 K-gluconate, 6 KCl, 10 HEPES, 0.2 EGTA, 5 Na_2-phosphocreatine, 2 Na_2ATP, 0.5 Na_2GTP, and 2 $MgCl_2$ (290–300 mOsm, pH adjusted to 7.2 with KOH); 0.1% biocytin was added for morphological analysis in a subset of experiments. Filled pipettes had a resistance of 3–7 MΩ. Membrane potential values given in the text are not corrected for the liquid junction potential.

Cells were visualized using infrared differential interference contrast video microscopy (BX-51WI, Olympus). The STN was identified as an almond-shaped structure in close proximity to the internal capsule and substantia nigra pars reticulata (SNr; Fig. 1*A*). Identification was confirmed by probing VGAT-YFP fluorescence in epifluorescence illumination using a 490 nm LED light source (Thorlabs). The STN was homogeneously YFP-negative, in contrast to the neighboring SNr.

We recorded from up to 7 cells simultaneously in depths of up to 72 μm beneath slice surface (mean ± SEM: 39 ± 1 μm; Fig. 1*B*). The series resistance in current-clamp recordings was compensated using the automated bridge balance compensation of the amplifier. Recordings were performed using 4 two-channel Multiclamp 700B amplifiers (Molecular Devices). Data were low-pass filtered at 6 kHz using the amplifiers built-in Bessel filter and digitized with a Digidata 1550 (Molecular Devices) at a sampling rate of 20 kHz. The pClamp 10.3.0.7 software package (Molecular Devices) was used for data acquisition and analysis. Recorded cells had a resting membrane potential of −60 ± 1 mV (mean ± SEM).

Synaptic connectivity screening. Trains of 4 action potentials (APs) at 20 Hz, a physiological burst frequency in the STN (Tinkhauser et al., 2017a), were elicited in a single cell by injecting 1- to 2-ms-long suprathreshold current pulses of 1–2.5 nA. Each recording sweep was 8 s long, and the individual cells were stimulated sequentially in 1 s intervals; therefore, each cell was activated once every 8 s (0.125 Hz). For the analysis of synaptic connectivity, 20–40 sweeps were averaged. All postsynaptic traces were thoroughly examined for postsynaptic potentials with a maximum latency of <3 ms to presynaptic APs, allowing for the detection of unitary postsynaptic potentials as small as 40 μV in average amplitude (Böhm et al., 2015; Peng et al., 2017).

Visualization of recorded neurons. After recording and concomitantly filling the cells with biocytin, slices were immersion-fixed in a solution containing 4% PFA and 4% sucrose in 0.1 M PB for a minimum of 12 h (overnight) at 4°C. Slices were then rinsed extensively in 0.1 M PB and subsequently permeabilized in a solution containing 0.3%–0.5% Triton X-100 in 0.1 M PB. Processed and biocytin-containing cells were visualized using avidin-conjugated AlexaFluor-647 (Thermo Fisher Scientific; dilution 1:500; RRID:AB_2336066) before being coverslipped using an aqueous mounting medium. Imaging of the slices was performed on a confocal laser-scanning microscope (Olympus FluoView FV1000) using a 4× objective for overview of cell clusters, and a 30× silicone-immersion objective (numerical aperture, 1.05) to obtain image stacks for the assessment of single-cell morphology. Fluorescence emission from YFP-labeled putative GABAergic cells was elicited by the 480 nm line of an Argon laser. A 643 nm laser diode was used to visualize the AlexaFluor-647 in biocytin-labeled neurons (Fig. 1*D*). Selected cells were morphologically reconstructed using the Simple Neurite Tracer plug-in (Longair et al., 2011) in the Fiji distribution of ImageJ software (National Institutes of Health; RRID:SCR_003070; Fig. 1*E*).

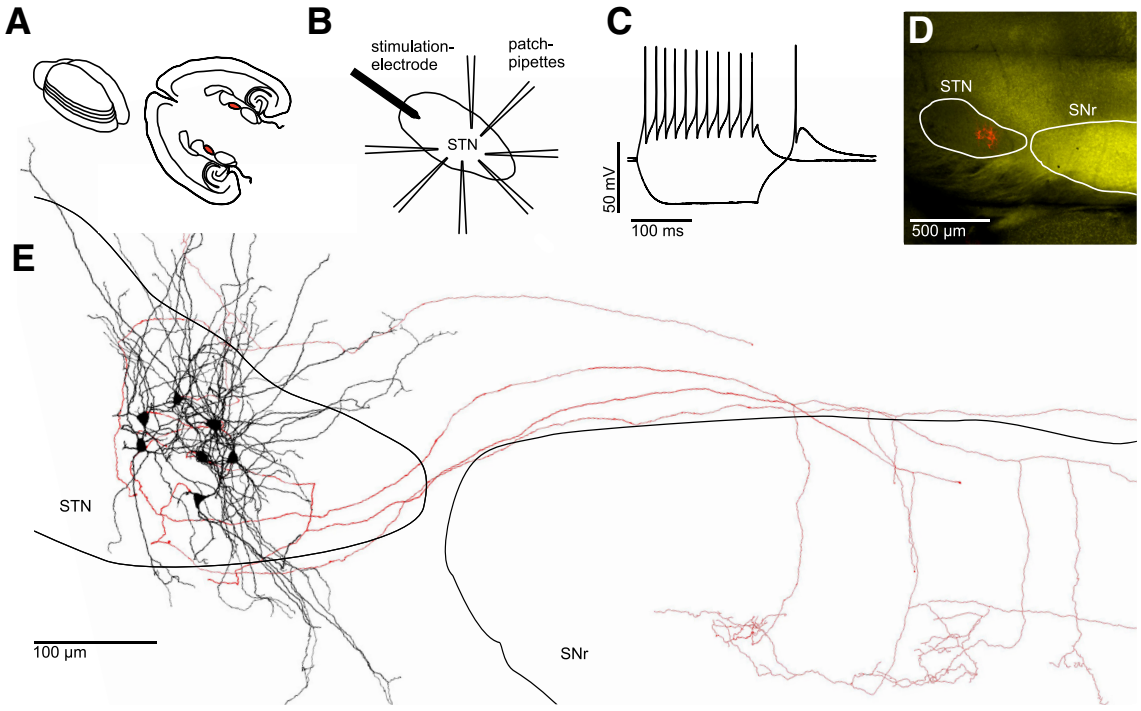

Figure 1. Electrophysiological and morphological characterization of clusters of neurons within the STN. ***A***, Left, Schematic drawing of an acutely isolated rat brain. Parallel lines indicate orientation of subsequently obtained "horizontal" slices. Right, Anatomical landmarks in a horizontal brain slice with the STN in each hemisphere highlighted in red. ***B***, Experimental paradigm: up to 7 STN neurons were recorded simultaneously. An extracellular stimulation electrode was placed at the rostral tip of the STN to stimulate axons afferent to the cluster of recorded neurons. ***C***, AP pattern of an STN neuron in response to a depolarizing current injection superimposed on a voltage trace in response to a hyperpolarizing current injection, which results in a rebound spike characteristic for STN neurons. ***D***, Fluorescence microscopic image of a horizontal slice obtained from a VGAT-YFP rat (see Materials and Methods) containing both the STN (VGAT-YFP-negative) and the SNr (VGAT-YFP-positive). Red-labeled structures in the STN represent seven simultaneously recorded and biocytin-filled neurons. ***E***, Reconstruction of the same cluster of neurons shown in ***D***. Black represents dendrites and somata. Red represents axons. Note the partially preserved axonal projections to the SNr.

Analysis of spatial proximities between STN neurons. Spatial proximities between pairs of recorded STN neurons were screened for using the ImageJ software. We examined confocal image stacks of 5 cell clusters from 5 animals. Potential contacts were classified as contacts originating from main axon segments or axon collaterals. Reconstructed cell pairs from recorded cell clusters were analyzed for potential contacts using a custom NEURON (https://neuron.yale.edu/neuron/) script. Number and dendritic length of potential contacts within 4 μm radius (center to center) from the central axis of the axon were determined per cell pair from the recorded clusters.

Placement of stimulation electrode/extracellular stimulation settings. For extracellular stimulation, a tungsten bipolar electrode (tip diameter ~30 μm) was placed in the rostral part of the STN (Fig. 1*B*). The electrode was lowered ~50 μm into the slice. Stimulation intensity varied between 8 and 500 μA across experiments, with a pulse duration of 100 μs.

Drugs. Drugs were purchased from Tocris Bioscience. Concentrated stock solutions of gabazine (GABA-A-receptor antagonist), D-AP5, and CNQX disodium salt (ionotropic glutamate-receptor antagonists) were made with H_2O and diluted in ACSF immediately before use for bath application at final concentrations of 10, 50, and 10 μM, respectively.

Minimal stimulation paradigm. Stimulation intensity was increased in steps of 10 μA until a postsynaptic response was seen in one of several simultaneously recorded cells, and subsequent stimulation intensity adjusted in steps of 1 μA to precisely determine the minimal stimulation threshold. Divergence of afferents onto STN neurons within a recorded cluster was studied by assessing the parallel emergence of postsynaptic responses in simultaneously recorded cells. To study GABAergic transmission in more detail, glutamatergic transmission was blocked in a subset of experiments using D-AP5 and CNQX. Glutamatergic transmission was studied in isolation in the presence of gabazine.

Single-pulse stimulation. Single stimulation pulses of up to 500 μA were applied without pharmacological manipulation to cause broad afferent activation and reveal the degree of overlay of GABAergic and glutamatergic synaptic responses within single cells and across a recorded cluster. Experiments were performed both in voltage- and current-clamp mode to study synaptic inputs and AP generation in STN neurons, respectively. In each experiment, we recorded 10 sweeps to screen signal variability. To disentangle AP generation in STN neurons from the influence of afferent GABAergic activity, experiments were performed in the presence of gabazine in a subset of experiments. While most experiments were performed at resting membrane potential, some cells were depolarized to −60 or −50 mV (in both the gabazine and nongabazine condition) to facilitate AP generation. Whenever single-pulse stimulation evoked APs in one of the recorded cells, we evaluated the first AP after stimulus. In a next step, we compared cell-specific median latencies and SDs of APs. SDs were omitted whenever less than two APs were recorded. On a group level, we compared between the gabazine and nongabazine condition across cells.

Variation of extracellular stimulation frequency. To study frequency-dependent dynamics of synaptic inputs to STN neurons, stimuli of 500 μA were applied at 10, 20, and 130 Hz. Each stimulation train was applied for 1 s, and the stimulation interval was followed by a 4 s break. Thus, the total sweep duration was 5 s. A total of 10 sweeps were recorded for each stimulation frequency and averaged for subsequent analysis. Experiments with clear and reliable onset of synaptic responses (either compound glutamatergic or compound GABAergic) in all tested stimulation frequencies were included in further *post hoc* analysis. In a subset of experiments, it was necessary to extrapolate the stimulation artifact offset toward baseline to correctly assess EPSC or IPSC amplitude. To quantify and normalize synaptic depression for individual cells, we calculated synaptic depression ratios dividing the synaptic current amplitude evoked by the fifth stimulus by the synaptic current amplitude evoked by the first stimulus. To quantify synaptic recovery after DBS-like stimulation frequencies of 130 Hz, we compared synaptic current amplitudes after the first stimulus in the first sweep to their counterparts in the 10th sweep.

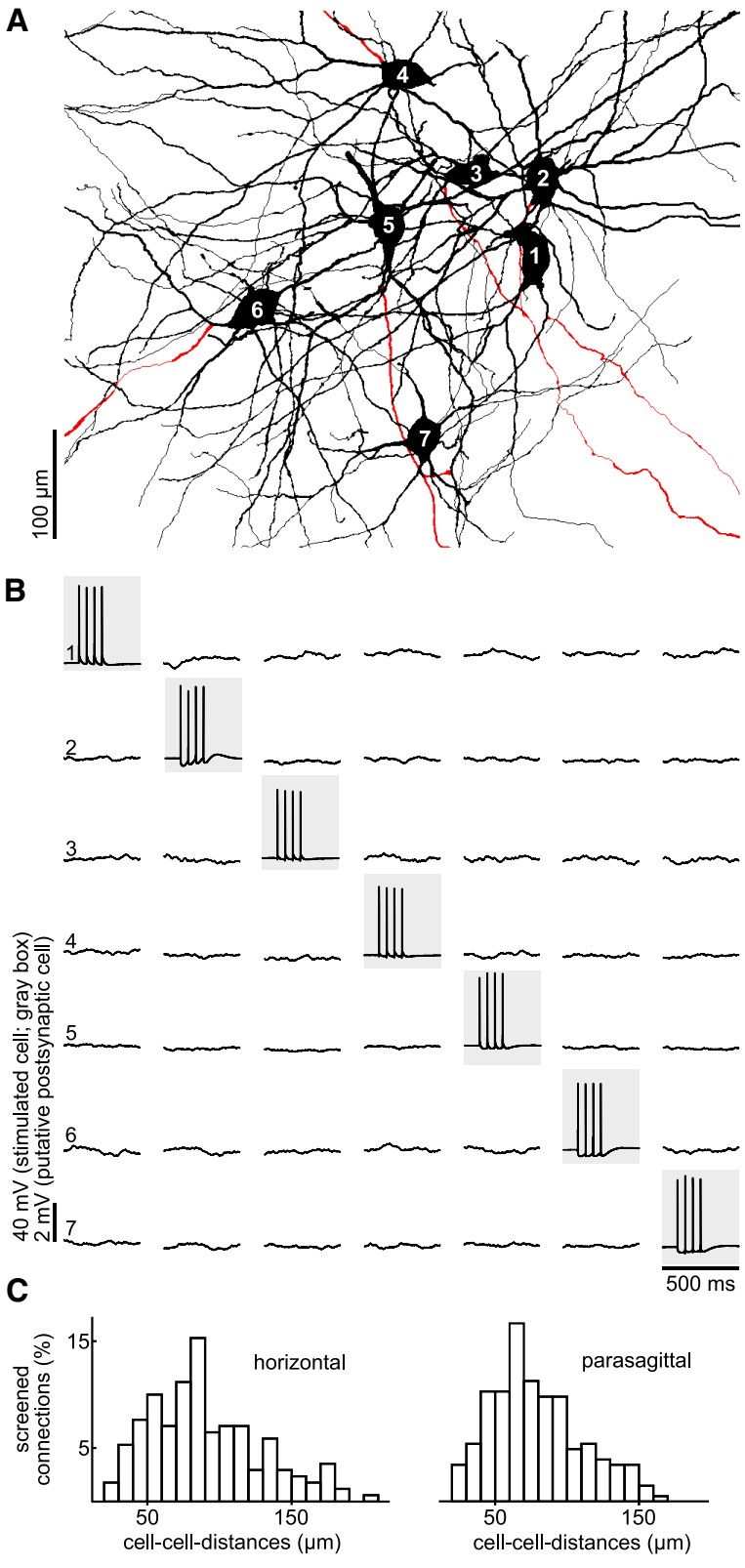

Figure 2. Simultaneous recordings of up to 7 STN neurons show no mutual synaptic connectivity. ***A***, Reconstruction of simultaneously recorded STN neurons (different cluster than in Fig. 1). ***B***, Connectivity screening of the set of cells in ***A***. Neurons are stimulated consecutively to generate a burst of four APs (gray boxes). Recordings of the other, potentially postsynaptic, neurons are shown in the respective column as averages of 40 sweeps. Note the complete lack of AP-evoked unitary postsynaptic potentials. ***C***, Distributions of distances between tested pairs of neurons in horizontal and parasagittal slices.

Statistical analysis. Statistical analyses were performed in Excel (Microsoft; RRID: SCR_016137) and MATLAB (The MathWorks; RRID:SCR_001622). Data are presented as the median and interquartile range, unless otherwise stated. Boxplots (central line, median; box, 25%–75%; maximal whisker length, 2 times the interquartile range; data points beyond the whiskers displayed using "+") are used to illustrate sample distributions. Group data were compared using nonparametric Wilcoxon signed-rank test and Mann–Whitney *U* test for paired and nonpaired comparisons, respectively. Multiple comparisons were corrected for by multiplying *p* values by the number of comparisons (Bonferroni correction). Final *p* values <0.05 were considered significant.

Results

Multipatch experiments reveal no synaptic interconnectivity between simultaneously recorded STN neurons

To probe intranuclear mutual connectivity between STN neurons, we performed multiple whole-cell recordings from local clusters of up to 7 neurons simultaneously (Fig. 2*A*), allowing us to test up to 42 possible synaptic connections at once (Fig. 2*B*). Using this approach, we examined a total of 830 connections between STN neurons in the juvenile cohort: 418 of those in slices cut in the parasagittal plane and 412 in the horizontal plane. Intersomatic distances between recorded cells ranged between 20 and 208 μm (Fig. 2*C*). The connectivity analysis was extended to an adult cohort to control for age-dependent effects, whereby an additional 44 synaptic connections were tested. In none of the tested connections did an AP in a putative presynaptic cell result in a temporally correlated postsynaptic potential in a simultaneously recorded cell, indicating a lack of functional connectivity between STN neurons.

To assess the morphological characteristics of the recorded cells, a subset of neurons were intracellularly filled, visualized, and reconstructed (38 STN cells in 7 clusters). Examined STN neurons had homogeneous morphological characteristics, featuring an ovoid soma and a bipolar dendritic tree with 4–6 primary dendrites (median: 5). Dendrites were aspiny, extended up to a distance of 322.2 μm (272.5 to 393 μm) from the soma, and had a total length of 2191 μm (median; 1768–2865 μm). Somatodendritic domains were restricted to the STN, although occasionally individual dendrites were observed to extend outside the nucleus for shorter distances. For 27 neurons, an axon could be unequivocally identified. Most

cells showed a typical axonal morphology as previously described for STN projection neurons (Koshimizu et al., 2013): a thick initial segment followed by a T-shaped bifurcation with the secondary axon branches projecting rostrally and caudally, respectively (16 cells; Figs. 1*E*, 3). In some of these neurons ($n = 8$), the caudal axon branch could be followed as far as the SNr within the slice. In a few neurons (6 cells), local axonal collaterals were observed. The number of collaterals emerging from the primary and secondary axon was, however, low, and they showed little further branching (median number of collateral branches per cell was 3; 1–5). Therefore, the extent of the axon local collaterals remained limited with a total length of 368 μm (median; 315–659 μm, 6 cells).

As the possibility of intranuclear synaptic contacts has been raised by previous anatomical studies (Hammond and Yelnik, 1983; Kita et al., 1983; Chang et al., 1984; Ammari et al., 2010; Gouty-Colomer et al., 2018), we examined the overlap of dendritic and axonal arborizations of the recorded neurons. Visual inspection revealed axo-dendritic proximities between neuron pairs of the recorded and visualized STN clusters (Fig. 3). To systematically analyze the existence of such potential contacts, axons and dendrites of the reconstructed cells were examined pairwise for locations of close proximity (see Materials and Methods). In 50 of 84 cell pairs examined, a total of 91 axo-dendritic proximities was found. Of these, 79 involved a primary axon and 12 small-caliber axon collaterals. Axo-dendritic proximities were found mostly proximally on the potential postsynaptic cell at a median distance of 87 μm (41–146 μm, 91 potential contacts) measured along the dendrites from the soma. In addition, we also observed 12 axo-axonic proximities in 8 of the 84 examined cell pairs. Thus, the overlap of axonal and dendritic arbors and the existence of proximities between neurites of STN cells suggest that an anatomical potential of intranuclear connectivity exists; however, these spatial proximities do not translate into functional synaptic connections between the cells.

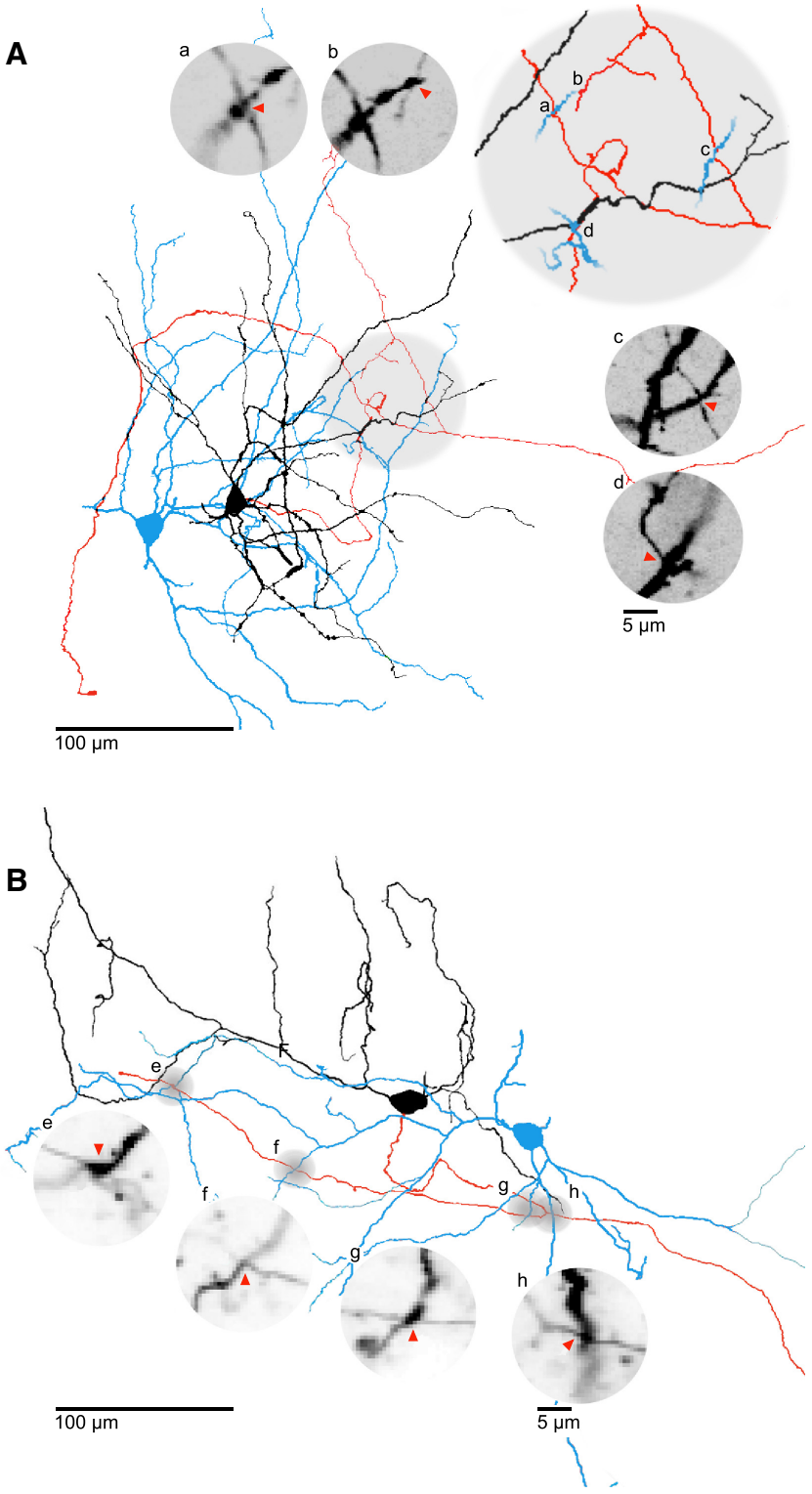

Figure 3. Local axo-dendritic proximities between neurons of the STN. ***A***, ***B***, 2D representations of reconstructed STN neurons with axo-dendritic proximities. Soma and dendrites of putative presynaptic cells (black) and their axons (red); blue represents putative postsynaptic cells. Gray circles represent site of proximity. Insets, Confocal *z* stack close-ups of the proximities. Letters a–h show corresponding sites in 2D representations of reconstructed neurons. Red arrows indicate potential contact site. The cells in panel ***A*** are taken from the cluster displayed in Figure 1*E*.

Minimal stimulation experiments demonstrate sparse projections by incoming afferent fibers onto local clusters of STN neurons

To study functional connectivity of afferents to STN neurons and in particular their divergence, we next applied extracellular stimulation while recording in voltage-clamp mode from clusters of STN neurons (Fig. 4). The stimulating electrode was placed in the rostral end of the STN, where afferents enter the nucleus (Kita and Kita, 2012; Mallet et al., 2012). To activate single afferent axons, we applied a minimal stimulation protocol, and divergence was assessed by the number of simultaneously appearing

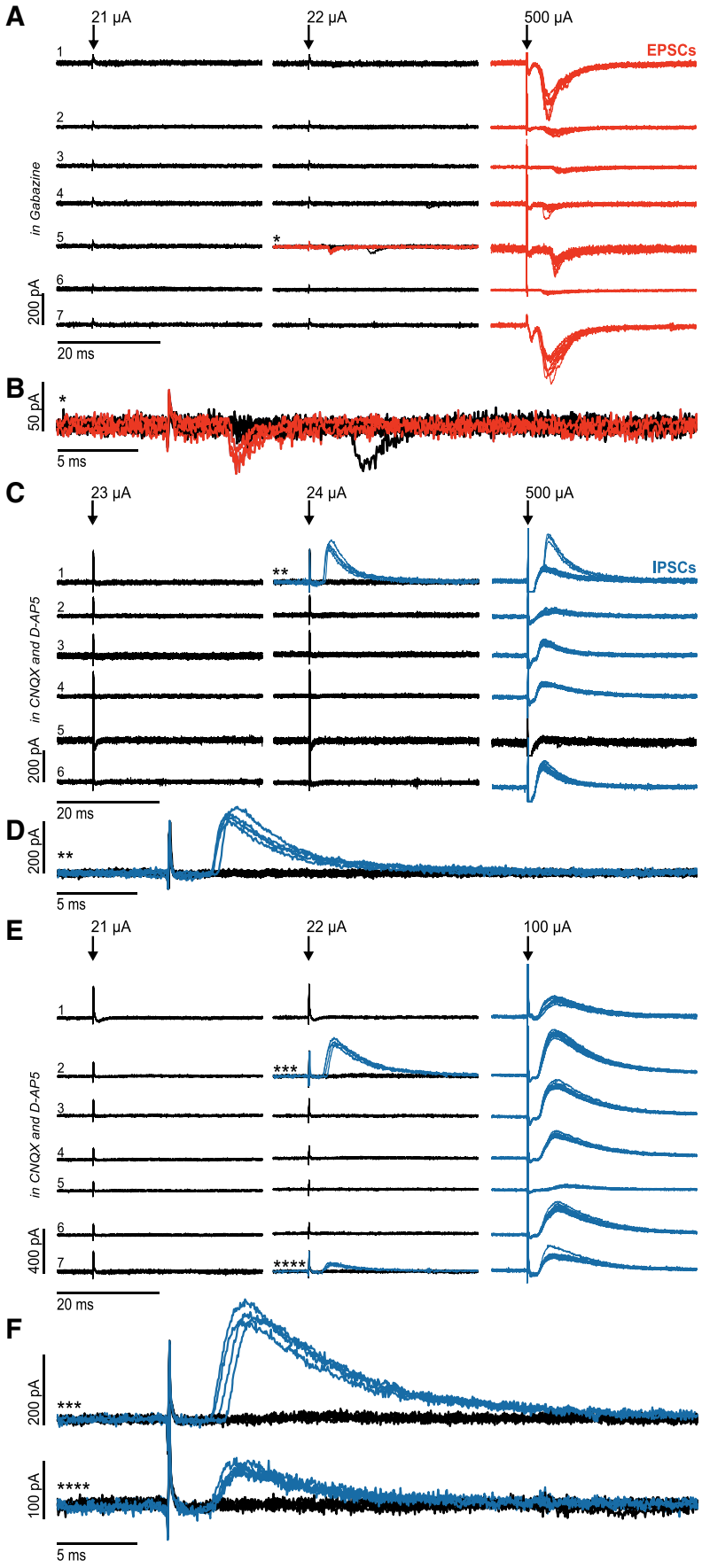

Figure 4. Minimal stimulation experiments reveal a low divergence of glutamatergic and GABAergic projections to local clusters of STN neurons. ***A***, Minimal stimulation of afferents to a cluster of STN neurons in the presence of the $GABA_A$-R blocker gabazine. *First neuron of the cluster that displayed evoked postsynaptic currents. Red represents traces in which evoked postsynaptic currents were detected. ***B***, Enlarged traces from neuron 5 (*) in ***A***. ***C***, Minimal stimulation of afferents to a cluster of STN neurons in the presence of CNQX and D-AP5 (glutamate-receptor blockers). **First neuron of the cluster that displayed evoked postsynaptic currents. Blue represents traces in which evoked postsynaptic currents were detected. ***D***, Enlarged traces from neuron 1 (**) in ***C***. ***E***, Minimal stimulation of afferents to a cluster of STN neurons in the presence of CNQX and D-AP5 (glutamate-R blockers). Parallel appearance of two inhibitory synaptic inputs (***, ****). Blue represents traces in which evoked postsynaptic currents were detected. ***F***, Enlarged traces from neuron 2 (***) and neuron 7 (****) in ***E***.

synaptic inputs in cells of the recorded cluster (see Materials and Methods). Given our finding of absent intranuclear connectivity, responses to intranuclear stimulation should reflect the activation of projections to the nucleus.

In all cell clusters tested, the excitatory synaptic input was detected in only one of the recorded neurons at minimal stimulation intensity, and this was independent of the slice orientation (horizontal plane: 4 clusters; cluster sizes: 7, 7, 7, and 6 cells; parasagittal plane: 4 clusters; cluster sizes: 7, 7, 7, and 6 cells; Fig. 4*A*,*B*), indicating a very low divergence of the input fibers. When stimulation intensity was subsequently increased, synaptic inputs were also recorded in other cells of the respective cluster, confirming that these cells also received afferent synaptic inputs; however, these can be assumed to be mediated by distinct afferent fibers.

This observation was replicated for the GABAergic input in the presence of CNQX and APV: in 7 of 10 clusters tested, only a single cell showed inhibitory synaptic responses at threshold stimulation intensity (horizontal plane: 4 clusters, cluster sizes: 7, 7, 6, and 5 cells; parasagittal plane: 3 clusters, cluster sizes: 5, 5, and 5 cells; Fig. 4*C*,*D*). However, in 3 further clusters, postsynaptic currents were recorded in two neurons at the minimal stimulation intensity (horizontal plane: 2 clusters, cluster sizes: 7 and 4 cells; parasagittal plane: 1 cluster, cluster size: 6 cells; Fig. 4*E*,*F*), reflecting that a sparse divergence of afferent fibers may exist.

GABAergic responses were elicited with short latency (2.81 ms, 2.22–3.75 ms, $n = 13$) in the presence of AMPA- and NMDA-receptor blockers, making polysynaptic activation unlikely. There was no difference between synaptic latencies of glutamatergic responses (2.81 ms, 2.34–4.0 ms, $n = 8$) and GABAergic responses. Thus, it is highly likely that both the IPSCs

and the EPSCs were monosynaptic. Furthermore, synaptic amplitudes of the glutamatergic responses were in a remarkably narrow range (27.5 mA, 24.75–31.5 mA, $n = 8$), consistent with their single contact-mediated, monosynaptic nature. GABAergic inputs, in contrast, had large amplitudes with higher variability (47 mA, 22.38–110.63 mA, $n = 13$). This finding is consistent with previously reported sparsely distributed terminal clusters of GABAergic afferent input to the STN that form multiple synaptic contacts onto individual STN neurons (Baufreton et al., 2009).

In summary, this suggests that both glutamatergic and GABAergic incoming fibers to the nucleus provide a sparse and selective, rather than a broad and divergent, input onto local clusters of STN neurons.

Costimulation of inhibitory and excitatory afferents delays and disperses AP generation in STN neurons

To investigate the joint effect of convergent glutamatergic and GABAergic afferents, large-intensity extracellular stimuli were applied (see Materials and Methods). The simultaneous activation of the sparse projections produced compound postsynaptic currents in individual STN neurons (Fig. 5). Within the same cell cluster, however, neurons showed diverse synaptic responses predominantly glutamatergic, GABAergic, or mixed (Fig. 5*B*).

To study the timing of AP generation in STN neurons in response to these variable synaptic currents, we switched to the current-clamp mode (Fig. 5*C*). Under this condition, the same stimuli elicited APs in a subset of cells (32 of 142 neurons tested, 23%). In most cells, the APs had long latencies and showed high temporal dispersion (Fig. 5*C*). On the group level, the median latency was 20.2 ms (6.81–119.8 ms, $n = 32$), with a temporal dispersion of 7.24 ms (SDs across cells, 0.77–31 ms, $n = 28$).

To next examine APs evoked by the excitatory input in isolation, we bath-applied gabazine to block $GABA_A$ receptor-mediated synaptic components (Fig. 5*D*). This manipulation resulted in a recruitment of 32% of STN neurons (23 of 73 neurons tested). Compared with control, APs were elicited with markedly shorter latency (median latencies across cells: 7.3 ms, 4.53–8.6 ms, $n = 22$; $p = 0.002$) and lower temporal variability (SDs across cells: 0.46 ms, 0.12–1.11 ms, $n = 18$; $p = 0.002$).

In summary, excitatory afferents alone drive STN neurons with short latency and low temporal variability. In contrast, costimulation of inhibitory afferents delays and disperses AP generation in STN neurons. Thus, the interaction of simultaneously recruited glutamatergic and GABAergic inputs can desynchronize neurons of the STN.

Repetitive DBS-like stimulation produces differential short-term depression of glutamatergic and GABAergic inputs to the STN

In view of the tight interplay of glutamatergic and GABAergic inputs in the recruitment of STN neurons, we next aimed to study the dynamics of these two afferent systems during repetitive stimulation. We applied 1 s trains of extracellular stimuli at low (10 and 20 Hz) and high, DBS-like frequencies (130 Hz) while recording from the cell clusters (Fig. 6). As described above, the compound synaptic responses were variable across the cells of the recorded clusters. Nevertheless, both compound glutamatergic and GABAergic synaptic responses showed short-term depression during the stimulus train.

For low-stimulation frequencies, synaptic depression was comparable for compound excitatory and compound inhibitory responses. At 10 Hz, the synaptic depression ratio (fifth/first synaptic amplitude) for EPSCs was 0.44 (0.4–0.55, $n = 12$) and for IPSCs 0.58 (0.55–0.62, $n = 9$; $p = 0.27$ for EPSCs vs IPSCs). At 20 Hz, the depression ratio for EPSCs was 0.32 (0.3–0.54, $n = 12$) and for IPSCs 0.58 (0.5–0.62, $n = 9$; $p = 0.46$ for EPSCs vs IPSCs; Fig. 6*A*). The synaptic depression ratios were not significantly different between 10 Hz and 20 Hz stimulation neither for compound EPSCs ($p = 0.61$) nor for IPSCs ($p = 1$). However, DBS-like high-frequency stimulation at 130 Hz caused a dramatic decrease of the EPSC amplitude over the train resulting in a depression ratio of 0.07 (0.03–0.13, $n = 12$; Fig. 6*B*,*C*). Comparing the degree of depression of EPSCs, the difference was highly significant between 130 Hz and 10 Hz ($p = 0.004$) or 20 Hz ($p = 0.004$), respectively (Fig. 6*D*). In contrast, the IPSCs showed only moderate depression even at high frequencies (ratio of 0.46, 0.4–0.48, $n = 9$; $p = 0.001$ for EPSCs vs IPSCs) and no statistical differences when comparing stimulation frequencies of 130 Hz versus 10 Hz ($p = 0.07$) or 20 Hz ($p = 0.18$; Fig. 6*D*).

Despite strong synaptic depression during the stimulation train, both EPSCs and IPSCs rapidly recovered after a 4 s break (Fig. 6*E*). Synaptic amplitudes in response to the first stimulus in the trains showed no significant difference between the first and the 10th repetition either for EPSCs (first: −78 pA, −118 to −62 pA; 10th: −85 pA, −125 to −52 pA, $n = 12$; $p = 0.57$) or for IPSCs (first: 109 pA, 67 to 226 pA; 10th: 130 pA, 75 to 237 pA, $n = 9$; $p = 0.91$; Fig. 6*F*).

In summary, the degree of synaptic depression does not differ between compound glutamatergic and GABAergic synaptic inputs for low-stimulation frequencies. However, at high, DBS-like frequencies, the compound glutamatergic drive rapidly and almost completely depresses after only a few stimuli in the train. In contrast, the GABAergic input remains relatively robust at a moderate level of depression. Thus, the differential dynamics of STN inputs will cause a major shift in the balance of excitation and inhibition toward inhibition.

Discussion

In our study, focusing on the synaptic connectivity of the STN, we found no evidence for intranuclear mutual connections between STN neurons in acute slices of juvenile and adult rats. We observed sparse divergence of individual afferent fibers of both glutamatergic and GABAergic input onto neurons of the recorded clusters when tested by a minimal stimulation protocol. Recruitment of pharmacologically isolated glutamatergic afferents at higher stimulus intensities evoked short-latency, highly synchronous APs, whereas costimulation of glutamatergic and GABAergic afferents resulted in delayed and dispersed AP generation in STN neurons. Finally, repetitive extracellular stimulation at high, DBS-like frequencies, but not at low frequencies, produced differential short-term plasticity of glutamatergic and GABAergic inputs, due to a dramatic reduction of excitatory but not inhibitory responses. Thus, DBS-like stimulation patterns can dynamically shift the balance of synaptic excitation and inhibition in the STN toward inhibition.

Sparse afferent and absent intrinsic connectivity of the STN

The rat STN is considered to comprise a homogeneous population of glutamatergic neurons. Nevertheless, features of GABAergic transmission in a subset of STN neurons have previously been reported despite predominant evidence for their glutamatergic phenotype (Jin et al., 2011). Lévesque and Parent (2005) further suggested that the human STN contains GABAergic interneurons. The lack of vGAT-YFP expression and the homogeneity of morphological properties in our sample do not support the existence of GABAergic neurons in the

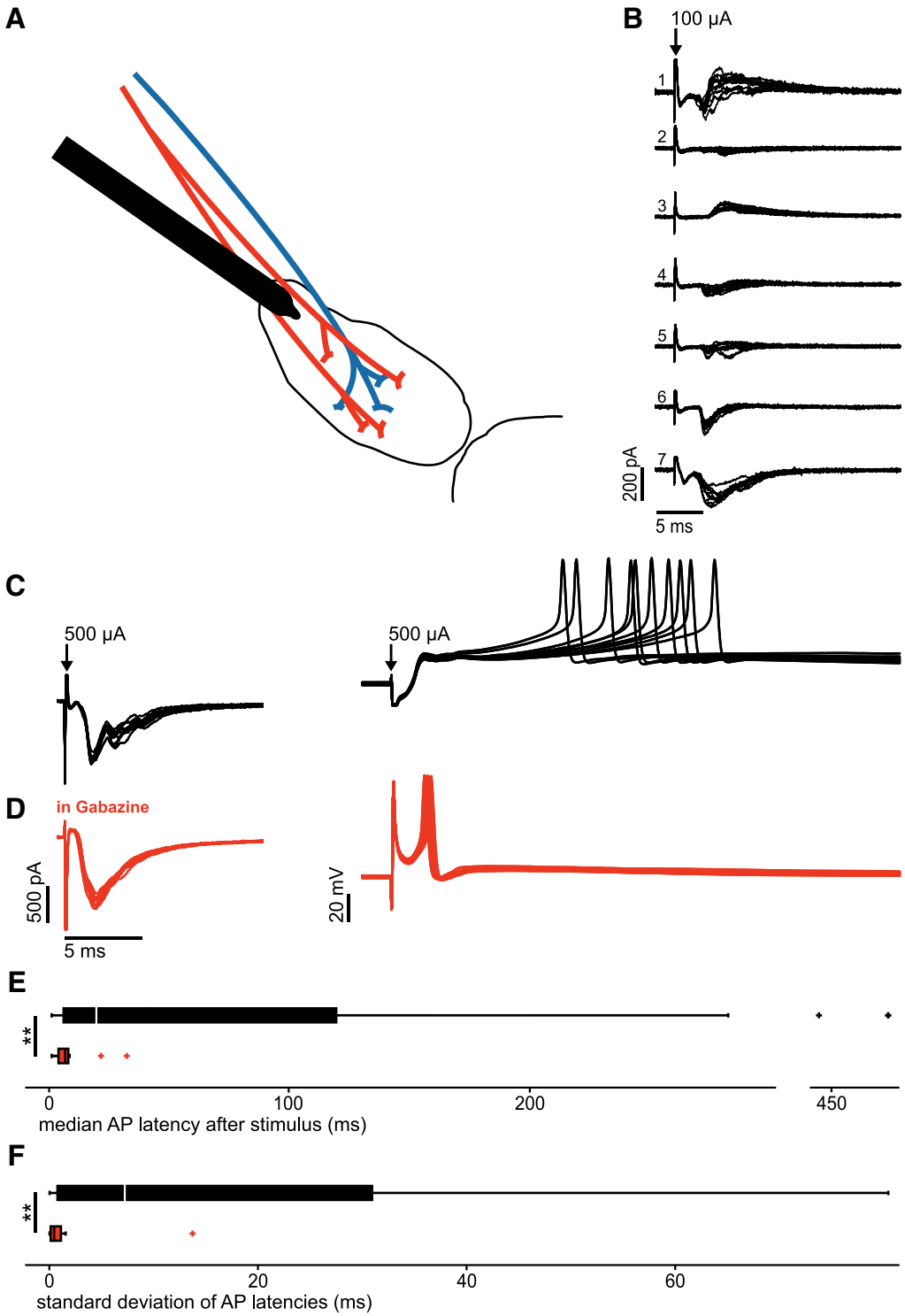

Figure 5. GABAergic costimulation delays and desynchronizes AP generation in STN neurons. ***A***, Schematic drawing of experimental paradigm. Red represents glutamatergic afferents to the STN. Blue represents GABAergic afferents to the STN. ***B***, Example traces of compound glutamatergic, GABAergic, and mixed compound synaptic currents in a cluster of STN neurons. ***C***, Voltage-clamp and current-clamp recordings of an individual STN neuron. ***D***, Voltage-clamp and current-clamp recordings of the same STN neuron as in ***C*** in the presence of gabazine. ***E***, Boxplots displaying the distribution of the medians of AP latency following a single stimulus as exemplified in ***C*** and ***D***. Top, $n = 32$ neurons without synaptic blockers (black). Bottom, $n = 22$ in the presence of gabazine (red). **Highly significant difference ($p < 0.01$). ***F***, Boxplots displaying the distribution of SDs of AP latency after a single stimulus as exemplified in ***C*** and ***D***. Top, $n = 28$ neurons without synaptic blockers (black). Bottom, $n = 18$ in the presence of gabazine (red).

rat STN. This question, however, would need further investigation and the possibility of interspecies differences has to be acknowledged.

Intranuclear mutual connectivity between glutamatergic STN neurons has been proposed to be of crucial importance for computational function and to contribute to neural synchrony in this nucleus (Gillies and Willshaw, 2004; Shen and Johnson, 2006; Ammari et al., 2010). Convergently, anatomical studies demonstrated local axon collaterals of STN neurons (Hammond and Yelnik, 1983; Kita et al., 1983; Chang et al., 1984; Ammari et al.,

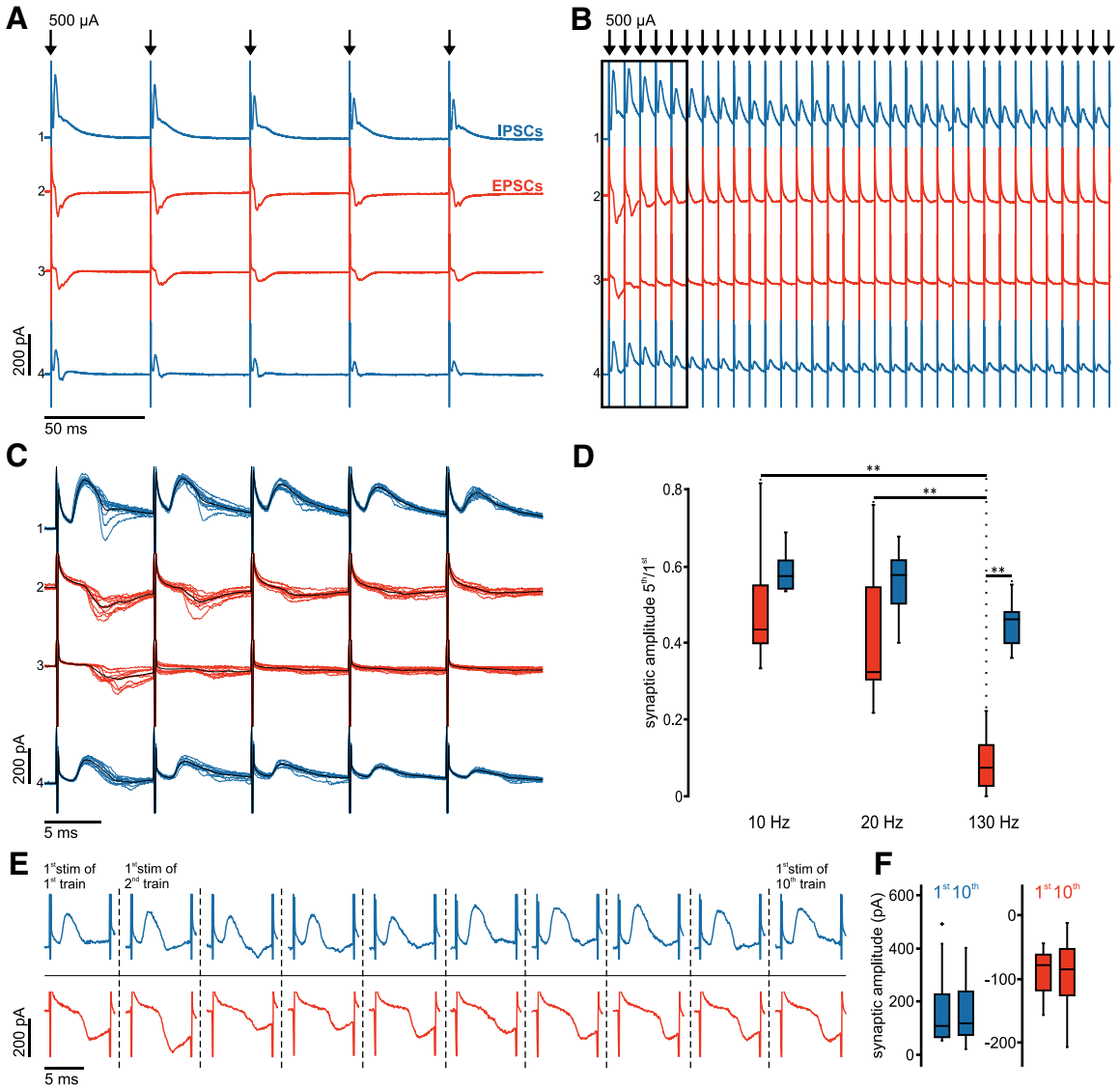

Figure 6. Sustained inhibition during DBS-like stimulation contrasts rapid depression of excitatory inputs. ***A***, Averaged voltage-clamp traces at 20 Hz stimulation frequency in four simultaneously recorded STN neurons. ***B***, Averaged voltage-clamp traces from the same STN neurons as in ***A*** at 130 Hz stimulation frequency. ***C***, Same traces as in ***B*** (black frame), albeit as single sweeps at higher temporal resolution; the respective average traces are superimposed in black. ***D***, Group data ($n = 12$ compound, predominantly glutamatergic EPSCs: red boxes; and $n = 9$ compound, predominantly GABAergic IPSCs: blue boxes) show distribution of synaptic depression ratios (fifth/first) for the respective stimulation frequencies. **Highly significant difference ($p < 0.01$). ***E***, Representative traces show the synaptic responses evoked by the first pulses of the 10 consecutive 130 Hz stimulus trains. Blue represents compound, predominantly GABAergic IPSCs. Red represents predominantly glutamatergic EPSCs. ***F***, Summary box charts show the peak amplitudes of the first synaptic responses in the first and 10th stimulation trains. Blue represents compound, predominantly GABAergic IPSCs ($n = 9$). Red represents compound, predominantly glutamatergic EPSCs ($n = 12$).

2010; Gouty-Colomer et al., 2018), interpreted as indication of local synaptic connections. Consistently, we found axon collaterals, albeit with a limited extent, for a subset of STN neurons. We also observed proximities between axons and dendrites of STN neurons. Results of our extensive multiple whole-cell recordings, however, revealed no functional connectivity between any of the closely spaced neuron pairs examined. Thus, the putative anatomical contacts do not translate into discernible functional connectivity, making mutual synaptic connectivity between glutamatergic STN neurons unlikely. This is in good agreement with previous acute slice work that investigated synchrony in the STN (Wilson et al., 2004). Our results contrast those obtained in organotypic rat midbrain slice culture pointing to intranuclear excitatory connectivity (Chu et al., 2012), which, however, might be explained by extensive axonal sprouting in such preparations (Debanne et al., 1998). Local axon collaterals and axo-dendritic proximities may serve other functions, such as regulation of remote inputs, as suggested for striatal microcircuits (Du et al., 2017).

Combination of multiple recordings with minimal stimulation further allowed us to assess the divergence of afferent inputs to the STN. Our results reveal that both excitatory and inhibitory afferents show low divergence onto the closely spaced neurons of STN cell clusters. This finding is in good agreement with a previous study demonstrating a sparse and selective connectivity from the GPe onto STN neurons (Baufreton et al., 2009). Our results extend these findings by showing that glutamatergic projections exhibit a similar or even more selective projection pattern, in good agreement with previous anatomical data (Kita and Kita, 2012).

Both mutual intrinsic and divergent afferent connectivity may serve as anatomical substrates for the emergence of synchrony in a local neuronal network. Although we cannot fully rule out the

existence of recurrent excitatory connections in the STN, these must be of very low occurrence with minimal somatic effect. Furthermore, the afferent inputs, in particular the excitatory projections, show minimal divergence. Together, these features identify STN neurons as independent processing units, which integrate convergent sparse afferent inputs in a largely parallel manner. Synchrony in such a system will be inherited from upstream structures. Reciprocal interactions with the GPe may further endow the STN with pattern generation capabilities (Bevan et al., 2002). Because remote afferents take center stage for the synchronization in the STN, their interactions and dynamic properties are critical for synaptic control of the nucleus.

GABAergic coactivation desynchronizes STN neurons

Activation of the afferent input at higher stimulation intensities produced diverse patterns of compound synaptic currents across the neurons of the recorded clusters, reflecting the convergence of a varying composition of stimulated glutamatergic and GABAergic fibers onto the cells. While the convergent excitatory input in isolation was able to recruit STN neurons with short latency and high temporal precision, the costimulation of GABAergic fibers delayed and desynchronized APs under control conditions, as suggested by Bevan et al. (2007).

However, simultaneous convergent glutamatergic and GABAergic input is unlikely to occur under *in vivo* conditions. Still, the extracellular costimulation paradigm of excitatory and inhibitory afferents in our experiments might bear direct relevance for DBS in the clinical setting, which similarly activates a mixed population of afferent fibers (Reich et al., 2015). In PD, pallidal GABAergic transmission to the STN is increased (Fan et al., 2012; Chu et al., 2015) and phase-shifted (Mallet et al., 2008a,b) relative to synchronized motor cortex excitation (Goldberg et al., 2002). Importantly, out-of-phase inhibition, when preceding EPSPs, can support AP generation by increasing the availability of Na^+ channels (Baufreton et al., 2005). In an oscillatory context, when excitation and inhibition alternate in the cycle, inhibition can enhance the efficiency, precision, and ultimately the synchrony of spiking (Baufreton et al., 2005). Our results on the desynchronizing effect of GABAergic costimulation suggest that DBS inverts this synchronizing role of the GABAergic input. In forcing simultaneous activation of inhibitory and excitatory inputs, it is directly shunting and hyperpolarizing excitatory input, effectively closing the time window in which a synchronized afferent drive can recruit the STN.

Sustained inhibition contrasts rapid depression of excitatory inputs during high-frequency stimulation

The particular susceptibility of the glutamatergic drive to synaptic depression upon repetitive stimulation at high frequencies has further relevance for DBS. Previous studies have proposed short-term depression as a DBS mechanism of action (Zheng et al., 2011; Rosenbaum et al., 2014; Milosevic et al., 2018). Our results corroborate this finding: in contrast to stimulation at low frequencies, when glutamatergic and GABAergic inputs showed comparable degrees of depression, high frequencies produced a rapid and dramatic reduction in EPSCs, whereas IPSCs remain relatively robust, resulting in a shift toward inhibition. Noteworthy, the activation of inhibitory input during DBS has recently received attention (Chiken and Nambu, 2014), but has not been directly compared to DBS effects on excitatory inputs. The shift in the balance largely decouples the STN from its glutamatergic cortical drive, whereas the maintained inhibitory input promotes desynchronization. Thus, differential short-term depression of synaptic transmission represents a mechanism to attenuate the unpredictable variability of recruited afferent fibers.

From synaptic dynamics to therapeutic interventions

While the STN receives glutamatergic and GABAergic inputs, previous studies argued that the selective stimulation of the hyperdirect pathway alone could account for therapeutic effects of DBS (Gradinaru et al., 2009; Sanders and Jaeger, 2016). Both the therapeutic DBS effects observed in the aforementioned studies and the effects on glutamatergic afferent control presented in our study critically depend on stimulation frequency. Limiting the DBS mechanism of action to effects on the hyperdirect pathway, however, fails to explain why electrode placement in the GPi, a frequently used alternative target in PD which is not monosynaptically connected to the cortex, is comparable in its clinical effect (Follett et al., 2010; Williams et al., 2014). Indeed, recent studies suggest that GPi-DBS, similar to STN-DBS, is reducing cortical beta-gamma phase-amplitude coupling (Malekmohammadi et al., 2018), a previously reported biomarker of PD (de Hemptinne et al., 2013). Thus, it seems unlikely that the DBS mechanism of action is exclusively depending on selective stimulation of the hyperdirect pathway. Instead, electrical stimulation plausibly targets both GABAergic and glutamatergic fibers simultaneously. As both GPi and STN are similar in integrating GABAergic and glutamatergic inputs, differential short-term plasticity could provide a general, target-independent mechanism that prevents the downstream propagation of pathological activity.

Further, our results may shed light on the synaptic mechanisms underlying feedback-controlled intermittent forms of DBS (Little et al., 2013; Herz et al., 2018). These adaptive stimulation paradigms have been proposed to trim excessive synchronization at beta frequencies with high temporal precision (Ramirez-Zamora et al., 2017; Tinkhauser et al., 2017b). Our data suggest that the rapid depression of glutamatergic inputs and the promotion of desynchronizing afferent control complies with the necessity for fast, temporally precise disruption of local synchrony. Because synaptic recovery is complete within seconds, intermittent DBS allows for physiological synchronization dynamics in interstimulation intervals. In conclusion, the dynamic properties of afferent synapses revealed in this study fit well to intermittent stimulation paradigms, allowing for fast yet temporally restricted functional decoupling of the STN from synchronizing inputs.

References

Ammari R, Lopez C, Bioulac B, Garcia L, Hammond C (2010) Subthalamic nucleus evokes similar long lasting glutamatergic excitations in pallidal, entopeduncular and nigral neurons in the basal ganglia slice. Neuroscience 166:808–818.

Baufreton J, Atherton JF, Surmeier DJ, Bevan MD (2005) Enhancement of excitatory synaptic integration by GABAergic inhibition in the subthalamic nucleus. J Neurosci 25:8505–8517.

Baufreton J, Kirkham E, Atherton JF, Menard A, Magill PJ, Bolam JP, Bevan MD (2009) Sparse but selective and potent synaptic transmission from the globus pallidus to the subthalamic nucleus. J Neurophysiol 102:532–545.

Benabid AL, Pollak P, Gross C, Hoffmann D, Benazzouz A, Gao DM, Laurent A, Gentil M, Perret J (1994) Acute and long-term effects of subthalamic nucleus stimulation in Parkinson's disease. Stereotact Funct Neurosurg 62:76–84.

Bevan MD, Hallworth NE, Baufreton J (2007) GABAergic control of the subthalamic nucleus. Prog Brain Res 160:173–188.

Bevan MD, Magill PJ, Terman D, Bolam JP, Wilson CJ (2002) Move to the rhythm: oscillations in the subthalamic nucleus-external globus pallidus network. Trends Neurosci 25:525–531.

Böhm C, Peng Y, Maier N, Winterer J, Poulet JF, Geiger JR, Schmitz D (2015) Functional diversity of subicular principal cells during hippocampal ripples. J Neurosci 35:13608–13618.

Bolam JP, Hanley JJ, Booth PA, Bevan MD (2000) Synaptic organisation of the basal ganglia. J Anat 196:527–542.

Chang HT, Kita H, Kitai ST (1984) The ultrastructural morphology of the subthalamic-nigral axon terminals intracellularly labeled with horseradish peroxidase. Brain Res 299:182–185.

Chen CC, Brücke C, Kempf F, Kupsch A, Lu CS, Lee ST, Tisch S, Limousin P, Hariz M, Brown P (2006) Deep brain stimulation of the subthalamic nucleus: a two-edged sword. Curr Biol 16:R952–R953.

Chiken S, Nambu A (2014) Disrupting neuronal transmission: mechanism of DBS? Front Syst Neurosci 8:33.

Chu HY, Atherton JF, Wokosin D, Surmeier DJ, Bevan MD (2015) Heterosynaptic regulation of external globus pallidus inputs to the subthalamic nucleus by the motor cortex. Neuron 85:364–376.

Chu JU, Jeong MJ, Song KI, Lee HC, Kim J, Kim YJ, Choi K, Suh JK, Youn I (2012) Spontaneous synchronized burst firing of subthalamic nucleus neurons in rat brain slices measured on multi-electrode arrays. Neurosci Res 72:324–340.

Debanne D, Gähwiler BH, Thompson SM (1998) Long-term synaptic plasticity between pairs of individual CA3 pyramidal cells in rat hippocampal slice cultures. J Physiol 507:237–247.

de Hemptinne C, Ryapolova-Webb ES, Air EL, Garcia PA, Miller KJ, Ojemann JG, Ostrem JL, Galifianakis NB, Starr PA (2013) Exaggerated phase-amplitude coupling in the primary motor cortex in Parkinson disease. Proc Natl Acad Sci U S A 110:4780–4785.

Du K, Wu YW, Lindroos R, Liu Y, Rózsa B, Katona G, Ding JB, Kotaleski JH (2017) Cell-type-specific inhibition of the dendritic plateau potential in striatal spiny projection neurons. Proc Natl Acad Sci U S A 114:E7612–E7621.

Fan KY, Baufreton J, Surmeier DJ, Chan CS, Bevan MD (2012) Proliferation of external globus pallidus-subthalamic nucleus synapses following degeneration of midbrain dopamine neurons. J Neurosci 32:13718–13728.

Feingold J, Gibson DJ, DePasquale B, Graybiel AM (2015) Bursts of beta oscillation differentiate postperformance activity in the striatum and motor cortex of monkeys performing movement tasks. Proc Natl Acad Sci U S A 112:13687–13692.

Follett KA, Weaver FM, Stern M, Hur K, Harris CL, Luo P, Marks WJ Jr, Rothlind J, Sagher O, Moy C, Pahwa R, Burchiel K, Hogarth P, Lai EC, Duda JE, Holloway K, Samii A, Horn S, Bronstein JM, Stoner G, et al. (2010) Pallidal versus subthalamic deep-brain stimulation for Parkinson's disease. N Engl J Med 362:2077–2091.

Gillies A, Willshaw D (2004) Models of the subthalamic nucleus: the importance of intranuclear connectivity. Med Eng Phys 26:723–732.

Goldberg JA, Boraud T, Maraton S, Haber SN, Vaadia E, Bergman H (2002) Enhanced synchrony among primary motor cortex neurons in the 1-methyl-4-phenyl-1,2,3,6-tetrahydropyridine primate model of Parkinson's disease. J Neurosci 22:4639–4653.

Gouty-Colomer LA, Michel FJ, Baude A, Lopez-Pauchet C, Dufour A, Cossart R, Hammond C (2018) Mouse subthalamic nucleus neurons with local axon collaterals. J Comp Neurol 526:275–284.

Gradinaru V, Mogri M, Thompson KR, Henderson JM, Deisseroth K (2009) Optical deconstruction of parkinsonian neural circuitry. Science 324:354–359.

Hammond C, Yelnik J (1983) Intracellular labelling of rat subthalamic neurones with horseradish peroxidase: computer analysis of dendrites and characterization of axon arborization. Neuroscience 8:781–790.

Herz DM, Little S, Pedrosa DJ, Tinkhauser G, Cheeran B, Foltynie T, Bogacz R, Brown P (2018) Mechanisms underlying decision-making as revealed by deep-brain stimulation in patients with Parkinson's disease. Curr Biol 28:1169–1178.e6.

Jin XT, Galvan A, Wichmann T, Smith Y (2011) Localization and function of GABA transporters GAT-1 and GAT-3 in the basal ganglia. Front Syst Neurosci 5:63.

Kita H, Chang HT, Kitai ST (1983) The morphology of intracellularly labeled rat subthalamic neurons: a light microscopic analysis. J Comp Neurol 215:245–257.

Kita T, Kita H (2012) The subthalamic nucleus is one of multiple innervation sites for long-range corticofugal axons: a single-axon tracing study in the rat. J Neurosci 32:5990–5999.

Koshimizu Y, Fujiyama F, Nakamura KC, Furuta T, Kaneko T (2013) Quantitative analysis of axon bouton distribution of subthalamic nucleus neurons in the rat by single neuron visualization with a viral vector. J Comp Neurol 521:2125–2146.

Kühn AA, Kempf F, Brücke C, Gaynor Doyle L, Martinez-Torres I, Pogosyan A, Trottenberg T, Kupsch A, Schneider GH, Hariz MI, Vandenberghe W, Nuttin B, Brown P (2008) High-frequency stimulation of the subthalamic nucleus suppresses oscillatory beta activity in patients with Parkinson's disease in parallel with improvement in motor performance. J Neurosci 28:6165–6173.

Lévesque JC, Parent A (2005) GABAergic interneurons in human subthalamic nucleus. Mov Disord 20:574–584.

Li Q, Ke Y, Chan DC, Qian ZM, Yung KK, Ko H, Arbuthnott GW, Yung WH (2012) Therapeutic deep brain stimulation in parkinsonian rats directly influences motor cortex. Neuron 76:1030–1041.

Little S, Pogosyan A, Neal S, Zavala B, Zrinzo L, Hariz M, Foltynie T, Limousin P, Ashkan K, FitzGerald J, Green AL, Aziz TZ, Brown P (2013) Adaptive deep brain stimulation in advanced Parkinson disease. Ann Neurol 74:449–457.

Longair MH, Baker DA, Armstrong JD (2011) Simple neurite tracer: open source software for reconstruction, visualization and analysis of neuronal processes. Bioinformatics 27:2453–2454.

Malekmohammadi M, AuYong N, Ricks-Oddie J, Bordelon Y, Pouratian N (2018) Pallidal deep brain stimulation modulates excessive cortical high beta phase amplitude coupling in Parkinson disease. Brain Stimul 11:607–617.

Mallet N, Pogosyan A, Márton LF, Bolam JP, Brown P, Magill PJ (2008a) Parkinsonian beta oscillations in the external globus pallidus and their relationship with subthalamic nucleus activity. J Neurosci 28:14245–14258.

Mallet N, Pogosyan A, Sharott A, Csicsvari J, Bolam JP, Brown P, Magill PJ (2008b) Disrupted dopamine transmission and the emergence of exaggerated beta oscillations in subthalamic nucleus and cerebral cortex. J Neurosci 28:4795–4806.

Mallet N, Micklem BR, Henny P, Brown MT, Williams C, Bolam JP, Nakamura KC, Magill PJ (2012) Dichotomous organization of the external globus pallidus. Neuron 74:1075–1086.

Milosevic L, Kalia SK, Hodaie M, Lozano AM, Fasano A, Popovic MR, Hutchison WD (2018) Neuronal inhibition and synaptic plasticity of basal ganglia neurons in Parkinson's disease. Brain 141:177–190.

Mirzaei A, Kumar A, Leventhal D, Mallet N, Aertsen A, Berke J, Schmidt R (2017) Sensorimotor processing in the basal ganglia leads to transient beta oscillations during behavior. J Neurosci 37:11220–11232.

Nambu A, Tokuno H, Takada M (2002) Functional significance of the cortico-subthalamo-pallidal 'hyperdirect' pathway. Neurosci Res 43:111–117.

Neumann WJ, Degen K, Schneider GH, Brücke C, Huebl J, Brown P, Kühn AA (2016) Subthalamic synchronized oscillatory activity correlates with motor impairment in patients with Parkinson's disease. Mov Disord 31:1748–1751.

Peng Y, Barreda Tomás FJ, Klisch C, Vida I, Geiger JR (2017) Layer-specific organization of local excitatory and inhibitory synaptic connectivity in the rat presubiculum. Cereb Cortex 27:2435–2452.

Ramirez-Zamora A, Giordano JJ, Gunduz A, Brown P, Sanchez JC, Foote KD, Almeida L, Starr PA, Bronte-Stewart HM, Hu W, McIntyre C, Goodman W, Kumsa D, Grill WM, Walker HC, Johnson MD, Vitek JL, Greene D, Rizzuto DS, Song D, et al. (2017) Evolving applications, technological challenges and future opportunities in neuromodulation: Proceedings of the Fifth Annual Deep Brain Stimulation Think Tank. Front Neurosci 11:734.

Reich MM, Steigerwald F, Sawalhe AD, Reese R, Gunalan K, Johannes S, Nickl R, Matthies C, McIntyre CC, Volkmann J (2015) Short pulse width widens the therapeutic window of subthalamic neurostimulation. Ann Clin Transl Neurol 2:427–432.

Rosenbaum R, Zimnik A, Zheng F, Turner RS, Alzheimer C, Doiron B, Rubin JE (2014) Axonal and synaptic failure suppress the transfer of firing rate oscillations, synchrony and information during high frequency deep brain stimulation. Neurobiol Dis 62:86–99.

Sanders TH, Jaeger D (2016) Optogenetic stimulation of cortico-subthalamic projections is sufficient to ameliorate bradykinesia in 6-OHDA lesioned mice. Neurobiol Dis 95:225–237.

Shen KZ, Johnson SW (2006) Subthalamic stimulation evokes complex EPSCs in the rat substantia nigra pars reticulata in vitro. J Physiol 573:697–709.

Smith Y, Bolam JP, Von Krosigk M (1990) Topographical and synaptic organization of the GABA-containing pallidosubthalamic projection in the rat. Eur J Neurosci 2:500–511.

Steiner LA, Neumann WJ, Staub-Bartelt F, Herz DM, Tan H, Pogosyan A, Kühn AA, Brown P (2017) Subthalamic beta dynamics mirror parkinsonian bradykinesia months after neurostimulator implantation. Mov Disord 32:1183–1190.

Stephenson-Jones M, Samuelsson E, Ericsson J, Robertson B, Grillner S (2011) Evolutionary conservation of the basal ganglia as a common vertebrate mechanism for action selection. Curr Biol 21:1081–1091.

Tinkhauser G, Pogosyan A, Tan H, Herz DM, Kühn AA, Brown P (2017a) Beta burst dynamics in Parkinson's disease OFF and ON dopaminergic medication. Brain 140:2968–2981.

Tinkhauser G, Pogosyan A, Little S, Beudel M, Herz DM, Tan H, Brown P (2017b) The modulatory effect of adaptive deep brain stimulation on beta bursts in Parkinson's disease. Brain 140:1053–1067.

Uematsu M, Hirai Y, Karube F, Ebihara S, Kato M, Abe K, Obata K, Yoshida S, Hirabayashi M, Yanagawa Y, Kawaguchi Y (2008) Quantitative chemical composition of cortical GABAergic neurons revealed in transgenic venus-expressing rats. Cereb Cortex 18:315–330.

Williams NR, Foote KD, Okun MS (2014) STN vs. GPi deep brain stimulation: translating the rematch into clinical practice. Mov Disord Clin Pract 1:24–35.

Wilson CL, Puntis M, Lacey MG (2004) Overwhelmingly asynchronous firing of rat subthalamic nucleus neurones in brain slices provides little evidence for intrinsic interconnectivity. Neuroscience 123:187–200.

Zheng F, Lammert K, Nixdorf-Bergweiler BE, Steigerwald F, Volkmann J, Alzheimer C (2011) Axonal failure during high-frequency stimulation of rat subthalamic nucleus. J Physiol 589:2781–2793.

(10) CURRICULUM VITAE

My curriculum vitae does not appear in the electronic version of this dissertation for reasons of data protection.

My curriculum vitae does not appear in the electronic version of this dissertation for reasons of data protection.

My curriculum vitae does not appear in the electronic version of this dissertation for reasons of data protection.

(11) PUBLICATION LIST

Steiner, L.A., Barreda Tomás, F.J., Planert, H., Alle, H., Vida, I., Geiger, J.R.P. (2019), Connectivity and Dynamics Underlying Synpatic Control of the Subthalamic Nucleus. **Journal of Neuroscience,** 39:2470-2481. doi:10.1523/JNEUROSCI.1642-18.2019.

Impact factor: 5.97

Steiner, L.A., Neumann, W., Staub-Bartelt, F., Herz, D.M., Tan, H., Pogosyan, A., Kuhn, A.A. and Brown, P. (2017), Subthalamic Beta Dynamics Mirror Parkinsonian Bradykinesia Months After Neurostimulator Implantation. **Movement Disorders**, 32: 1183-1190. doi:10.1002/mds.27068.

Impact factor: 8.32

(12) ACKNOWLEDGEMENTS

This research was conducted at the Institute of Neurophysiology, Charité – University Medicine Berlin. I want to use this opportunity to thank the members of the Institute, my fellow PhD students, other colleagues and mentors, but also friends and family who have supported me throughout the years.

First and foremost, I would like to thank my primary supervisor Prof. Dr. rer. nat. Jörg R.P. Geiger. His support was and continues to be the base of my scientific training and his methodological and conceptual guidance has shaped my understanding of good scientific practice.

I also want to express my profound thanks to PD Dr. med. Henrik Alle. In particular, I want thank him for his extraordinary introduction to the field of Experimental Neurophysiology, his technical support with the implementation of my experimental paradigm and the many fruitful discussions on basal ganglia physiology.

Furthermore, I would like to thank Prof. Dr. med. Imre Vida, Federico J. Barreda Tomás and Dr. Henrike Planert for the very productive and smooth collaboration leading to the successful publication.

A big thank you to all the other members of the Institute of Neurophysiology. I fondly remember my time in the lab and want to thank everybody for the shared enthusiasm. I owe special thanks to Dr. med. Yangfan Peng, who has designed the multi-patch setup, thus providing essential technical prerequisites for this study. In addition, I want to thank my fellow PhD students Vera Wuntke, Michael Hadler, Franz X. Mittermeier, Julia Neugebauer and Ali Rifat for the mutual support in the lab and the helpful feedback in the past years.

My scientific training has also been influenced by discussions within the *clinical research unit 247: deep brain stimulation - mechanisms of action, cortex-basal ganglia physiology, therapy optimization*. In particular, I am thankful for the ongoing support of Prof. Dr. med. Andrea A. Kühn, who has given me the opportunity to participate in her research projects in Berlin and Oxford.

Last, but by far not least, I want to express deepest gratitude to my family, my parents Gabriele Ruth Steiner and Wolf-Emanuel Linsenhoff and my brother, Oliver Leopold Steiner, for all their encouragement.